PONTIFICIA UNIVERSIDAD CATOLICA DE CHILE
SCHOOL OF ENGINEERING

ON THE DYNAMICS OF GÖRTLER VORTICES OVER A CONCAVE SAND BED

BORIS CAMILO RODRÍGUEZ CORNEJO

Thesis submitted to the Office of Research and Graduate Studies
in partial fulfillment of the requirements for the degree of
Master of Science in Engineering

Advisor:
CRISTIAN ESCAURIAZA MESA

Santiago de Chile, August 9*th*, 2011

PONTIFICIA UNIVERSIDAD CATOLICA DE CHILE
SCHOOL OF ENGINEERING

ON THE DYNAMICS OF GÖRTLER VORTICES OVER A CONCAVE SAND BED

BORIS CAMILO RODRÍGUEZ CORNEJO

Members of the Committee:
CRISTIAN ESCAURIAZA MESA
RODRIGO CIENFUEGOS CARRASCO
ROBERT H.A. JANSSEN
JOSÉ RICARDO PÉREZ CORREA

Thesis submitted to the Office of Research and Graduate Studies
in partial fulfillment of the requirements for the degree of
Master of Science in Engineering

Santiago de Chile, August 9*th*, 2011

Gratefully to my family,

my friends

and Jazmin

ACKNOWLEDGEMENTS

I would like to thank my advisor Cristian Escauriaza for his guidance and support. It was a privilege and a great experience work with him; his motivation, creativity and intelligence were always present in this work. I would also like to express my gratitude to the members of my committee: Ricardo Pérez, Rodrigo Cienfuegos and Robert Janssen and professor Fotis Sotiropoulos for them support and comments to my work. In addition, I would like to thank to professors Bernardo Dominguez and Bonifacio Fernandez from Hydraulic and Environmental Engineering Department of Catholic University, who inspired me as student and engineer.

So many friends that I would like to thank. My friends from San Fernando, Santiago and other remote places were all very important to keep the right way. I would like to thank to the Student Chapter of Hydraulic and Environmental Engineering Department, thanks for them support and friendship, and good luck with thesis and research proyects.

I would like to thank, the people most important in my life: the family, specially to my parents for their unconditional love. They are who most appreciate this work and who "less understand it". I would like to dedicate this work and say thanks to Jazmin. She has been the emotional support of this work.

Finally, I want to thank the Arturo Cousiño Lyon scholarship and the financial aid provided by the FONDECYT project 11080032. Computational resources were provided by the Minnesota Supercomputing Institute (MSI).

TABLE OF CONTENTS

LIST OF FIGURES

LIST OF TABLES

ABSTRACT

Erosion and sediment transport processes in rivers and channels usually take place in arbitrary geometries and occur in turbulent conditions at high Reynolds numbers. Coherent structures that emerge from large-scale instabilities can play a fundamental role in sediment transport, and in many cases they constitute the most important mechanism of bed-load transport and scour in non-equilibrium conditions. The recent experiments carried out by Hopfinger et al. (2004) and Albayrak et al. (2008) have shown that streamwise Görtler vortices have a considerable impact on sediment transport rates and scour produced by a wall-jet flow downstream of a sluice gate. Görtler vortices emerge in an advanced stage of scour due to the concave curvature of the bed inside the scour hole and their interaction with the bed increases the shear stress and itensifies bed-load transport. To understand better the relation between coherent structures and sediment transport, we carry out detached-eddy simulations (DES) of the flow studied by Albayrak et al. (2008). We reproduce the original experimental configuration, by discretizing the domain using body-fitted curvilinear grid with a total of 9.7 million nodes. Our simulations can resolve the coherent structures of the flow at $Re = 156,200$, and capture the dynamics of the Görtler vortices inside the scour hole. The model not only reproduces the unsteady flowfield, but also the dynamic features of the shear-stress induced by the Görtler vortices, which are responsible for the sediment streaks that appear on the bed. The model can therefore serve as a powerful tool to predict sediment transport and scour under non-equilibrium conditions.

Keywords: Fluid Dynamics, Turbulence, Sediment Transport, Detached-eddy Simulations (DES), Görtler vortices.

RESUMEN

Los procesos de erosión y transporte de sedimentos en cauces naturales ocurren generalmente en geometrías arbitrarias y complejas, y en flujos turbulentos a altos números de Reynolds. Estructuras coherentes que emergen de inestabilidades de escalas mayores pueden cumplir un rol fundamental en el transporte, y en muchos casos constituyen el principal mecanismo de transporte de fondo y socavación en condiciones de no equilibrio. Las experiencias recientes de Hopfinger et al. (2004) y Albayrak et al. (2008) han demostrado que vórtices de Görtler en el sentido del flujo tienen un considerable impacto en las tasas de transporte de sedimentos y en la socavación producida por un flujo tipo jet de pared, aguas abajo de una compuerta plana. Vórtices de Görtler se producen en un estado avanzado de de socavación debido a la curvatura cóncava del lecho dentro de la zona de socavación. La interacción de estos vórtices con el fondo incremetan los esfuerzos de corte e intensifican el transporte de fondo. Para comprender de mejor forma la relación entre estructuras coherentes y transporte de sedimentos, realizamos simulaciones DES ("*detached-eddy simulations*") del flujo estudiado por Albayrak et al. (2008). Reproducimos la configuración original de los experimentos mediante la discretización del dominio, utilizando una grilla con coordenadas curvilíneas generalizadas con un total de 9.7 millones de nodos. Nuestras simulaciones son capaces de resolver las estructuras coherentes del flujo a número de Reynolds igual a $Re = 156,200$, y además capturan la dinámica de los vórtices de Görtler dentro de la zona de socavación. El modelo no solo reproduce el flujo no permanente, sino que además las características dinámicas de los esfuerzos de corte inducidos por los vórtices de Görtler, responsables de las líneas de surcos que aparecen en el lecho. Con estos resultados, el modelo puede servir como una herramienta poderosa para predecir el transporte de sedimento y la socavación bajo condiciones de no equilibrio.

Palabras Claves: Dinámica de Fluidos, Turbulencia, Transporte de Sedimentos, Simulaciones DES, Vórtices de Görtler.

1. INTRODUCTION

Sediment transport in nature is intimately connected to the dynamics of turbulent flows in aquatic environments. It is characterized by complex interactions that take place at the interface between the sediment surface and the flow, usually occurs in arbitrary complex geometries, and is further complicated by the varying properties of the sediment grains and the surrounding flowfield. Coherent structures in turbulent flows have a direct impact on the sediment transport and on the evolution of the bed topography in natural rivers and streams. The multiple scales within the turbulent flows interact with sediment particles, controlling erosion and deposition, and contribute to the development of dynamic patterns such as ripples and dunes that arise at multiple levels, up to the largest scales on the earth surface.

Due to the complexity of the sediment transport problem and in spite of the rapidly expanding body of literature dedicated to its study, there is still much to be done to understand and be able to model the sediment dynamics and the effects of the flow on sediment transport. However, with the help of powerful supercomputers it is now possible to investigate sediment transport processes through high resolution numerical simulations. Such simulations can be used to perform laboratory and field-scale experiments, and develop new theoretical and computational model for a broad range of engineering problems (Escauriaza, 2008; Paik et al., 2007, 2010; Escauriaza & Sotiropoulos, 2011c, 2011b).

The continuous growth of infraestructure and the social and environmental impacts of engineering projects in natural streams require a better understanding of the relation between the mechanisms of scour and turbulent flow to improve the design of hydraulic structures and reduce negative environmental burdens. Generally, the methods employed to predict and compute scour depths are empirical relations based on dimensional analysis and laboratory or field experiments (eg. Melville (1997)), which assume steady flow conditions and not give infomation about actual erosion mechanisms. Therefore, the modeling of three-dimensional turbulent flows has critical impact in understanding the physical that

govern the interaction of the flowfield with scour in order to get better hydraulic structure designs.

The main purpose of this investigations is study a particular coherent structure, so-called counter-rotating Görtler vortices, which have a direct impact on the increase of sediment transport rates (Hopfinger et al., 2004; Albayrak et al., 2008), by means of high resolution three-dimensional simulations.

These type of flows are highly three-dimensional, and characterized by a wide range of vortical scales that dominate sediment transport and erosion processes. These flows are further complicated when they interact with hydraulic structures, which produce unsteady vortices that emerge from flow instabilities, increasing the stresses on the bed and initiating local scour (Saric, 1994; Hopfinger et al., 2004; Albayrak et al., 2008).

These characteristics present a great challenge to numerical models intended to study the effects of unsteady coherent structures in sediment transport problems. At engineering scales, unsteady Reynolds-averaged Navier Stokes (URANS) models are usually employed to compute the mean flowfield, and account for the effects of the turbulence fluctuations by using a gradient-diffusion hypothesis to estimate the eddy-viscosity from transport equations. Recent investigations (Paik et al., 2007; Escauriaza & Sotiropoulos, 2011c) have demonstrated that URANS models fail to capture the unsteady features of flows driven by dynamically rich coherent structures, such as the horseshoe vortex system around obstacles mounted on the bed (Escauriaza & Sotiropoulos, 2011c). On the other hand, large eddy-simulations (LES) models can resolve the most important vortical structures in the flow, but they might become computationally expensive in complex flows at high Reynolds numbers in engineering applications. Recently, hybrid models such as detached-eddy simulations (DES) have shown to be powerful tools to resolve the large-scale coherent structures with moderate computational resources (Spalart et al., 1997; Spalart, 2009). DES combines the advantages of both, URANS and LES strategies, employing URANS models near solid walls, and LES in the rest of domain.

Clear examples on the importance of coherent structures arising from large-scales instabilities of the mean flow are the studies of Hopfinger et al. (2004) and Albayrak et al. (2008). These authors studied experimentally the scour produced by a wall-jet downstream of a sluice gate, and observed that the development of a concave bed surface due to the initial scour triggered a centrifugal instability, producing counter-rotating streamwise pairs of Görtler vortices inside the scour hole. These vortices played a significant role in the continuous development of scour as they generated high turbulent stresses and increased considerably the total sediment flux. Albayrak et al. (2008) performed statistical analyses of flow variables on a flat and concave walls, and observed experimentally for the second case the dynamic manifestation of streamwise Görtler vortices with a 3D acoustic profiler (ADVP).

In this chapter, the previous literature related to study of Görtler type flows and sediment transport modeling is reviewed to asses the current state of the art, and identify the challenges that will be addressed in this research.

1.1. Literature Review

Multiple studies have focused in the relation between the coherent structures of the flow and their interaction. Also, many studies have focused in centrifugal instabilities, especifically in Görtler vortices, which emerge by the instability of the turbulent boundary layer and the bed curvature inside the scour hole (Saric, 1994). This phenomenon arises as a consequence of the bed curvature and a velocity profile that decreases its magnitude with the radius of curvature. Several flows in these conditions have been thoroughly studied, such as Blasius velocity profiles or wall-jet profiles (Floryan, 1986). In the work of Hopfinger et al. (2004) it can be seen that this instability modifies the turbulent structure of the flow and substantially alters the sediment transport rate. Hopfinger et al. (2004) even reported the remarkable formation of sediment streaks due to the stresses generated by Görtler vortices. In their pioneering work, Hopfinger et al. (2004) also established rigorously the stability conditions of the wall-jet flow by performing an analysis based on the

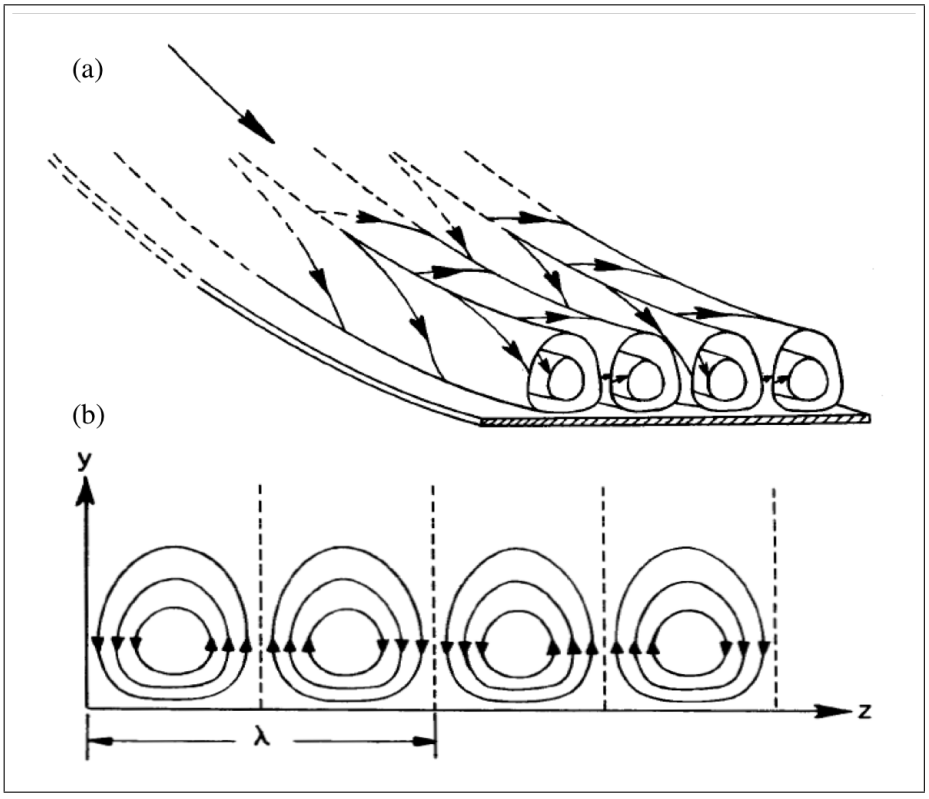

FIGURE 1.1. (a) Vortex disturbances in the flow of a fluid on a concave wall, axes of vorices parallel to principal flow direction. (b) Scheme of streamline pattern in a section at right angle to the principal flow direction.

turbulent Görtler number Tani (1962); Kobayashi and Fujisawa (1983), and used the experimental measurements to modify the erosion model of Hogg, Huppert, and Dade (1997). Studies about Görtler vortices and centrifugal instabilities have been focused on two areas: (1) Linear and Non-Linear Analysis using normal modes solutions and disturbance equations (Rintel, 1971; Aihara, 1976; Ragab & Nayfeh, 1981; Zebib & Bottaro, 1993) and (2) Experiments in curved wall-jet and film flows (Schweizer & Scriven, 1983; Saric, 1994; Matsson, 1995; Tandiono et al., 2008, 2009). Linear analysis was initiated by Görtler (1954) by means of a study of the stability of laminar boundary layer profiles on slightly curved walls relative to small disturbances, in the shape of vortices, whose axes are parallel to the principal direction of the flow, which are the so-called counter rotating Görtler vortices, as is shown in figure 1.1 .

Görtler (1954) in his study used a normal mode solution determining the next disturbance equation, where three velocity components and pressure are define as follows:

$$u = u_0(y) + u_1(y)\cos(\alpha z)\exp\{\beta t\} \tag{1.1}$$

$$v = v_1(y)\cos(\alpha z)\exp\{\beta t\} \tag{1.2}$$

$$w = w_1(y)\sin(\alpha z)\exp\{\beta t\} \tag{1.3}$$

$$p = p_0(y) + p_1(y)\cos(\alpha z)\exp\{\beta t\} \tag{1.4}$$

where $u_0(y)$ is a laminar boundary-layer basic flow formed by some previous history based on the viscosity effect or the undisturbed flow. α and β are real values, where $\alpha = \frac{2\pi}{\lambda}$, being λ the wave length of the disturbance. The quantity β governs the amplification or damping of the flow, depending upon whether it is greater or smaller than zero. The values of x, y, z are the cartesian coordinates and t is the temporal scale. The equation (1.4) corresponds to a vortex distribution at the curved wall, the axes of which coincide with the direction of the principal flow. Furtheremore, the numerical results of Görtler (1954) by means of this linear analysis in Navier-Stokes equations, yield information about stability limit with respect to dimensionless Görtler number, range of wave length of vortices that can be amplified, and about the most dangerous vortices with regard to the transition from laminar to turbulent flow. Görtler number is defined as:

$$G_\theta = \frac{U_m \theta}{\nu_t}\sqrt{\frac{\theta}{R}} \tag{1.5}$$

where U_m is the "constant" velocity in the outer region for a laminar boundary-layer flow, and the maxim velocity for a wall-jet flow. θ is the momentum thickness, ν_t is the eddy viscosity and *R* is the curvature radius. Finally, Görtler found that the critical conditions in terms of momentum thickness are insensitive to the analytic character of the velocity profile, but they are more sensitive to the presence of points of inflection (Görtler, 1954). Other studies on linear mathematical analysis, such as the study of Rintel (1971), were

applied to different velocity profiles and compared with experimental data. Rintel (1971) showed different critical values of the Görtler for different conditions on velocity profiles, such as the presence of points of inflection. Following with the studies of Görtler (1954) and Rintel (1971), Ragab and Nayfeh (1981) made a linear analysis for different velocity profiles such as Blasius profile, Falkner-Skan profile, and a flow velocity profile over a hump, in addition evaluated the effect of displacement thickness and the effect of decaying streamline curvature in critical values of Görtler number. Hall (1988, 1990) solved the non-linear parabolized equations in a spatial formulation and was able to calculate the distortion of the mean flow. Schweizer and Scriven (1983) found evidence of Görtler-type vortices in laminar flows and discussed the dependence of the wavelength of the instability on flow parameters. Matsson (1995) used a hot-wire anemometry and smoke visualizations to study the jet on a concave wall and found that streamwise vortices are amplified on the concave wall and that the growth of vortices is dependent on the initial amplitude, i.e. the highest initial amplitude gives the maximum strength of vortices. Tandiono et al. (2008, 2009) performed experiences in a 90 degrees curved Plexiglass test section connected to a low-speed, blow-down-type wind tunnel and found Görtler type vortices at curved position.

To our knowledge this Görtler centrifgual instability has never been captured and studied using high resolution unsteady 3D simulations, which constitute a novelty in this research field. The main objective of this research is to study the dynamics of Görtler vortices by carrying out DES simulations based on the experimental setup of Hopfinger et al. (2004) and Albayrak et al. (2008), for the turbulent flow in a scour-hole downstream of a sluice gate. The description of the flow and the experiences of Albayrak et al. (2008) are discussed in section 2. In section 3 we show the governing equations of the flow and describe the numerical model. Section 4 and 5 contain the principal results obtained from 3D simulations, compared with the observations of Hopfinger et al. (2004) and Albayrak et al. (2008). In section 6 we show the governing equations of a model of sediment transport which it is used for modeling sediment streaks reported by Hopfinger et al. (2004). The conclusions in section 7 summarize the results and outline future research.

2. EXPERIENCES OF HOPFINGER *ET AL.* AND ALBAYRAK *ET AL.*

Hopfinger et al. (2004) and Albayrak et al. (2008) performed laboratory experiments of a wall-jet flow coming from a sluice gate over an erodible sand bed in a rectangular channel. They studied the flowfield and the sediment erosion produced by Görtler vortices formed inside the scour hole that develops between the fixed bed channel and a downstream dune (see figure 2.1(a)). The experiments were conducted in a glass-side horizontal flume 17 m long, 0.5 m wide and 0.8 m deep (Albayrak et al., 2008). A sluice gate was installed at the middle of the channel, and the sand bed was located at a short distance from it ($L_f = 0.1$ m). The mobile bed was filled with uniformly graded sand of median grain diameter $d_{50} = 2$ mm, which constitutes a hydraulically rough surface. The downstream water depth was kept constant at $h_2 = 0.221$ m by adjusting a gate at the downstream end of the flume, and the upstream water depth h_1 was also maintained constant to produce a steady-state water discharge. The characteristic wall-jet velocity scale from the sluice gate is defined as $U_0 = \sqrt{2g\Delta h}$, where $\Delta h = h_2 - h_1$ with $h_1 = 0.247$ m and $h_2 = 0.221$ m (Albayrak et al., 2008). Using the downstream water depth as the length-scale, the Reynolds number of the flow is equal to $Re = 156,200$. It is important to note that the submerged hydraulic jump produced downstream the sluice gate does not alter the conditions of the free surface yielding a low Froude number of 0.1 in the section of the channel with sand bed.

At the beginning of the experiment the mobile bed was covered with a thin plate about 1 m long while water levels were adjusted to the desired values. At $t = 0$ the plate was removed and the erosion was initiated on the sediment bed. At time $t = t_s$, a quasi-steady-state with a maximum scour depth h_s was reached. This state is characterized by a very slow rate of erosion and sediment transport that is reached in a few hundred seconds after the experiment started. As depicted in figure 2.1, the bed exhibits a deep two-dimensional and concave scour hole. The curvature of the sand bed under these conditions is sufficiently high to trigger a centrifugal instability and generate Görtler vortices that dominate the transport of sediment and erosion, producing longitudinal bed forms in the slope region of the bed (Hopfinger et al., 2004). Albayrak et al. (2008) fixed the bed with the geometry

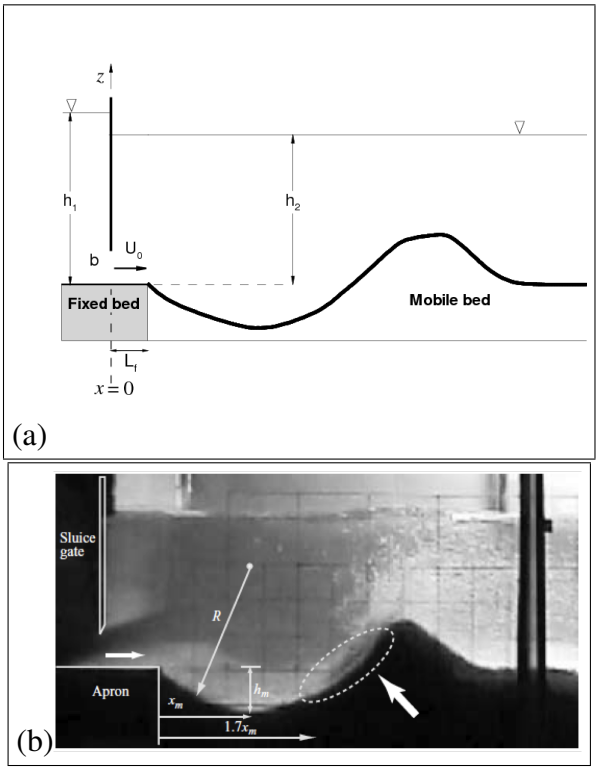

FIGURE 2.1. Schematic representation of the advanced scour conditions in the experiments carried out by Hopfinger *et al.* (2008). (a) Flow downstream of a sluice gate with an opening of $b = 0.05$ m, an apron of longitude $L_f = 0.1$ m and bulk velocity under the gate equal to $U_0 = 0.71$ m s^{-1}. (b) Picture obtained from experiences of Hopfinger *et al.* (2004).

produced by erosion under the quasi-steady-state conditions with $h_s = 0.064$ m, and performed detailed measurements with a three-dimensional acoustic Doppler velocity profiler (ADVP) to compute mean velocities and Reynolds stresses near the bed. Görtler vortices appeared randomly on the concave section of the bed and produced a series of upwash and downwash events in the instantaneous time-series of velocity in vertical planes across the bed, as later discussed. In this investigation we perform simulations for this condition of advanced quasi-steady erosion, for which the scour hole has a significante curvature and Görtler vortices appear. It is important to note that our simulations were conducted assuming that mobile bed is fixed to represent Görtler vortices and flow results. These results are the initial conditions for sediment transport modeling.

3. COMPUTATIONAL FLUID DYNAMICS MODEL

3.1. Governing equations

To simulate the flow downstream of the sluice gate (Hopfinger et al., 2004; Albayrak et al., 2008), we solve the three dimensional unsteady Reynolds-averaged Navier-Stokes equations (URANS) with a dual-time stepping artificial compresibility (AC) iteration scheme (Paik et al., 2007). The system of governing equations can be written in vector format for the generalized curvilinear coordinate system and in strong conservation form as follows,

$$\Gamma \frac{\partial Q}{\partial t} + J \frac{\partial}{\partial \xi^j} \left(F^j - F_v^j \right) = 0 \tag{3.1}$$

where

$$\Gamma = \mathrm{diag}\,[0\ 1\ 1\ 1]$$

$$Q = [P,\ u_1,\ u_2,\ u_3]^T$$

$$F^j = \frac{1}{J} \left[U^j, u_1 U^j + P\xi^j_{x_1}, u_2 U^j + P\xi^j_{x_2}, u_3 U^j + P\xi^j_{x_3} \right]^T$$

$$F_v^j = \frac{1}{J} \left(\frac{1}{Re} + \nu_t \right) \left[0, g^{mj} \frac{\partial u_1}{\partial \xi^m} + R_{m1}\xi^j_{x_m}, g^{mj} \frac{\partial u_2}{\partial \xi^m} + R_{m2}\xi^j_{x_m}, g^{mj} \frac{\partial u_3}{\partial \xi^m} + R_{m3}\xi^j_{x_m} \right]^T$$

In these equations *P* is the pressure divided by the density plus the diagonal component of the Reynolds stress tensor ($P = p + \frac{2}{3}k$), u_i ($i = 1, 2, 3$) are the Cartesian velocity components, x_i are the Cartesian coordinates, *J* is the Jacobian, $\xi^j_{x_i}$ are the metrics of the geometric transformation, U^j are the contravariant velocity components $U^j = u_i \xi^i_{x_j}$, g^{ij} are the components of the contravariant metric tensor $g^{ij} = \xi^i_{x_k} \xi^j_{x_k}$, Re is the Reynolds number, and the tensor R_{ij} is defined as: $R_{ij} = \dfrac{\partial u_i}{\partial \xi^k} \xi^k_{x_j}$. The Reynolds number of the flow is defined as $Re = \frac{U_0 h_2}{\nu}$ where U_0 is the velocity scale of the wall-jet, h_2 is the water depth downstream of the sluice gate, and ν is the kinematic viscosity of the fluid.

Since conventional URANS models to close equation (3.1) fail to capture the unsteadiness of coherent structures such as Görtler vortices, and full wall-resolving LES might need large computational resources for practical Reynolds numbers, we employ the DES approach, which is a hybrid URANS/LES turbulence model (Spalart et al., 1997; Spalart, 2009). The next section contains a complete explanation of turbulence models available and the one-equation eddy viscosity model adopted in the DES approach used in these simulations.

3.2. Statistical turbulence models

As previously discussed, realistic three-dimensional turbulent flows cannot be represented with DNS (direct numerical simulations) for all turbulent scales, and statistical turbulence models are employed to obtain numerical solutions of the governing equations (Pope, 2000). Statistical turbulence closures such as $k-\epsilon$, $k-\omega$, and one-equation Spallart-Allmaras (S-A), have been widely used to find the turbulent stresses in the URANS equations (Durbin & Petterson-Reif, 2001). Such models are practical from the computational standpoint but are rather diffusive and can only resolve the very largest scales of motion in turbulent flows (e.g. Ge and Sotiropoulos (2005)). For that the model utilized in this research is practical for engineering calculations at real-life Reynolds numbers *Re*, and can resolve dynamically rich coherent structures. Recent work (Paik & Sotiropoulos, 2005; Paik et al., 2007, 2009; Paik & Sotiropoulos, 2009; Escauriaza & Sotiropoulos, 2011c) has shown that hybrid URANS/LES models can serve this purpose. These turbulence models, such as detached-eddy simulations (DES) developed by Spalart et al. (1997), are combined formulations that compute the flow near solid walls in URANS mode, and resolve the eddies outside the boundary layer with LES. By eliminating the need of resolving near-wall turbulent eddies in a full LES models, hybrid formulations can resolve very rich dynamics in the flow at an affordable computational cost (Spalart, 2000).

The basic concept behind the URANS turbulence models is to express the Reynolds stress tensor in terms of mean-flow quantities. The Boussinesq approximation, employed

in isotropic turbulence models, assumes a linear relationship between the turbulent stresses and the mean strain-rate tensor,

$$-\left\langle u_i' u_j' \right\rangle = -\frac{2}{3} k \delta_{ij} + 2\nu_t S_{ij} S_{ij} \tag{3.2}$$

where the mean rate of strain is calculated as:

$$S_{ij} = \frac{1}{2}\left(\frac{\partial u_i}{\partial x_j} + \frac{\partial u_j}{\partial x_i}\right) \tag{3.3}$$

The graddient diffusion approximation of equation (3.2) introduces the turbulent eddy-viscosity ν_t to account for the effects of the smallest scales. The turbulent kinetic energy of these scales is *k*, and δ_{ij} is the Kronecker delta.

The turbulence model used in these simulations is the one-equation eddy viscosity model of Spalart and Allmaras (1994) (S-A) because of its simplicity, computational expedience, and great promise it has demonstrated in simulations of complex flows (Paik et al., 2007; Escauriaza & Sotiropoulos, 2011c). The S-A turbulence model (Spalart & Allmaras, 1994) is a one-equation closure for the URANS equations, and consists on a relation for the auxiliarity variable $\tilde{\nu}$ related to the eddy viscosity. This equation, derived from empirical arguments and dimensional analysis (Spalart, 2000), contains a destruction term that is a function of the distance from the wall and reduces the eddy viscosity ν_t inside the turbulent boundary layer. The model can be expressed in the curvilinear coordinate system as follows:

$$\frac{\partial \widetilde{\nu}}{\partial t} + J\frac{\partial}{\partial \xi^j}\left[F_t^j - F_{tv}^j\right] + J\, H_t = 0 \tag{3.4}$$

where

$$F_t^j = \frac{1}{J}\left[U^j \widetilde{\nu}\right]$$
$$F_{tv}^j = \frac{1}{J}\left[\frac{1}{\sigma}\left(\frac{1}{Re} + \widetilde{\nu}\right) g^{mj} \frac{\partial \widetilde{\nu}}{\partial \xi^m}\right]$$
$$H_t = \frac{1}{J}\left[-c_{b_1}\left(1 - f_{t_2}\right)\widetilde{S}\widetilde{\nu} + \left(c_{w_1} f_w - \frac{c_{b_1}}{\kappa^2} f_{t_2}\right)\left(\frac{\widetilde{\nu}}{d}\right)^2 - \frac{1}{\sigma} c_{b_2} g^{mj} \frac{\partial \widetilde{\nu}}{\partial \xi^m} \frac{\partial \widetilde{\nu}}{\partial \xi^m}\right]$$

The working variable $\tilde{\nu}$ in the S-A turbulence model has a direct relation to the turbulent eddy-viscosity, ($\tilde{\nu} = \nu_t / f_{v_1}$), and the destruction term contains the length scale d, which is defined as the distance from solid walls. In its extended version this model also includes transition terms, which provide a smooth transition from laminar to turbulent flow but they are not necessary in high Reynolds number flow studied in this research. The rest of the variables are defined by the following expressions,

$$f_{v_1} = \frac{\chi^3}{\chi^3 + c_{v_1}^3}, \qquad \chi = \frac{\tilde{\nu}}{\nu}, \qquad f_{t_2} = c_{t_3} \exp\left(-c_{t_4}\chi^2\right)$$

where ν is the molecular viscosity. In the production term, the modified vorticity $\tilde{S}$ is a function of the magnitude of the vorticty vector, $|S|$:

$$\tilde{S} = f_{v_3}|S| + \frac{\tilde{\nu}}{\kappa^2 d^2} f_{v_2}$$

The production term in this case is different from the original definition of Spalart and Allmaras (1994). We define the function f_{v_2} in terms of a new variable f_{v_3}, which prevents the spurious propagation of the eddy viscosity into attached laminar regions (Squires et al., 2005), such that:

$$f_{v_2} = \left(1 - \frac{\chi}{c_{v_2}}\right)^{-3}, \qquad f_{v_3} = \frac{\left(1 + \chi f_{v_1}\right)\left(1 - f_{v_2}\right)}{\chi}$$

The wall-destruction function is defined as,

$$f_w = g_0 \left[\frac{1 + c_{w_3}^6}{g_0^6 + c_{w_3}^6} \right]^{1/6}, \qquad g_0 = r + c_{w_2} \left(r^6 - r \right), \qquad r = \frac{\tilde{\nu}}{\tilde{S} \kappa^2 d^2} \tag{3.5}$$

Finally, we define the closure coefficients c_{b_1}, c_{b_2}, σ, c_{w_1}, c_{w_2}, c_{w_3}, c_{v_1}, c_{v_2}, and κ, which are constants, as follows:

$$\begin{gathered} c_{b_1} = 0.1355, \qquad \sigma = 2/3, \qquad c_{b_2} = 0.622, \qquad \kappa = 0.41 \\ c_{b_1} = \frac{c_{b_1}}{\kappa^2} + \frac{(1 + c_{b_2})}{\sigma}, \qquad c_{w_2} = 0.3, \qquad c_{w_3} = 2 \\ c_{v_1} = 7.1, \qquad c_{v_2} = 5, \qquad c_{t_3} = 1.1, c_{t_4} = 2 \end{gathered} \tag{3.6}$$

In its extended version this model also includes transitions terms, which provide a smooth transition from laminar to turbulent flow, but they are not necessary in the high Reynolds number simulations performed in this investigation.

In the hybrid DES approach developed by Spalart et al. (1997) the S-A turbulence model equation (3.4), functions as the subgrid scale (SGS) model of LES in regions away from the wall, where the grid density can resolve the scales of fluid motion near the size of the grid spacing. The modification to the S-A model to implement DES consists on replacing the distance to the nearest wall as the length-scale of the model by the following expression,

$$\tilde{d} \equiv \min \left(d, C_{DES} \Delta \right) \tag{3.7}$$

where $\Delta \equiv \max \left(\Delta x, \Delta y, \Delta z \right)$, is the largest dimension of the grid cell and the model constant is set equal to its standard value $C_{DES} = 0.65$, which was calibrated for homogeneous turbulence (Shur et al., 1999).

The transition of the model from URANS to LES is therefore controlled by the grid spacing. If the computational grid is constructed such that the wall-parallel grid spacing is of the order of the boundary layer thickness, the S-A URANS model is retained throughout

the boundary layer, and the prediction of the boundary layer separation is determined in the URANS mode of DES. Far from the solid boundaries, the model becomes a SGS eddy-viscosity equation. When the production balances the destruction term of the model, the length scale in the LES region yields a Smagorinsky eddy-viscosity. Analogous to the classical LES formulation, the role of Δ is to allow the energy cascade down to a length scale proportional to the grid size, making a pseudo-Kolmogorov length-scale based on the eddy viscosity proportional to Δ.

This hybrid model combines the strenghts of URANS and LES using only one partial differential equation to model the Reynolds stresses. Since fully resolved LES are still too costly at the range of Reynolds numbers in real sediment transport and scour problems, we utilize DES that can capture the most-energetic coherent structures and predict the unsteadiness of the flow and stresses that cause transport and bed erosion (Paik et al., 2007; Escauriaza & Sotiropoulos, 2011c, 2011b).

In the standard DES approach the transition between the URANS and LES modes depends exclusively on the grid spacing. The model was developed with the idea that the grid spacing in the direction parallel to the wall must be greater that at least half the thickness of the boundary layer, otherwise grid-induced nonphysical separation arises in regions where the mesh spacing violates these conditions (Spalart et al., 1997).

For the rough-wall simulations performed in this investigation we also use the modification of the turbulence model proposed by Aupoix and Spalart (2003).

The AC form of the governing equations is discretized using a second-order-accurate finite-volume method on a non-staggered computational grid. The convective terms are discretized using the second-order accurate, upwind biased QUICK scheme, and central differencing is employed for the pressure gradients, viscous fluxes, and source terms in the turbulenc equation. The third-order fourth-difference artificial dissipation method of Sotiropoulos and Abdallah (1992) is employed for pressure to eliminate odd-even decoupling of the pressure field. The physical time derivatives are discretized with a three-point-backward Euler-implicit temporal-integration scheme. The discrete equations are

marched in time to advance the solution to the next time step by adopting the dual or pseudo-time-stepping method. The system of equations is integrated in pseudo-time using a pressure-based implicit pre-conditioner (Sotiropoulos & Constantinescu, 1997) enhanced with local time stepping and V-cycle multigrid acceleration (Paik et al., 2007; Escauriaza & Sotiropoulos, 2011c).

The present numerical method has been employed to carry out coherent-structure resolving simulations for a variety of complex turbulent flows across a wide range of Reynolds numbers, from $Re = 2 \times 10^4$ (Paik et al., 2009) to as high as 4.2×10^5 (Paik & Sotiropoulos, 2009), in conjuction with URANS models and various variants of the DES model. The original version of DES (Spalart et al., 1997) was used by Paik et al. (2004) and Paik and Sotiropoulos (2005, 2009) while modified versions of the original model were used by Paik et al. (2007, 2009) and Escauriaza and Sotiropoulos (2011c, 2011b, 2011a). In all of these studies, the accuracy of the numerical method was demonstrated by qualitative and quantitative comparisons with available experimental data, tipically in terms of mean flow quantities and turbulence statistics.

For the turbulent flow above the concave sand bed we scanned the scoured section of the channel from the experimental measurements of the quasi-steady state of erosion measured by Albayrak et al. (2008) and perform an initial URANS simulation with an overset grid layout using a total of 6.0 million grid nodes, incorporating the entire length of the upstream channel used in the experiment, and the flow through the sluice gate as depicted in figure 3.1(b). As previously discussed, the URANS simulation cannot resolve the unsteady near-bed flow or capture the complex and rich dynamics of the Görtler vortices. To reduce the computational cost and concentrate our analysis in the concave bed, we simulate in more detail the flow over the sediment bed carrying out DES with its original formulation in a section that considers exclusively the scoured bed in the channel as shown in computational mesh shown in figure 3.1, maintaining a grid resolution of $y^+ \leq 0.5$ at wall boundaries. At the inlet we prescribe the converged URANS of the upstream rectangular channel and no-slip boundary condition is applied to all solid walls. A rigid-lid assumption is employed at the free surface due to the low-Froude number of the original

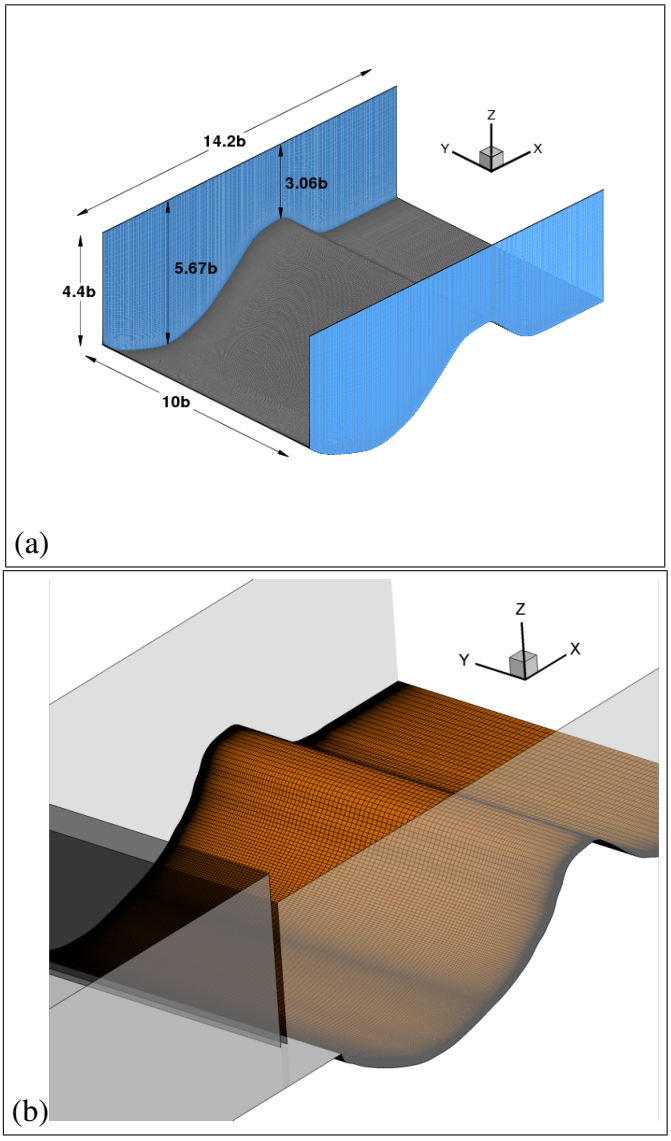

FIGURE 3.1. (a) Computational domain used in the DES computations for the fixed concave sand bed. The geometrical details are expressed in terms of the sluice gate opening, $b = 0.05$ m. Note that in this case the mesh is considerably finer with a total of 9.7 million grid nodes, with 209, 521 and 89 nodes in the i, j and k-directions respectively. (b) Three-dimensional layout of the computational domain for the numerical simulations.

experiments (Albayrak et al., 2008), and all the results presented in the following sections are obtained by using a non-dimensionl physical time-step of $\Delta t = 0.005$. In what follows we analyse the instantaneous three-dimensional flowfield in the concave sand bed, studying the instantaneous velocities and computing statistics of the resolved flow.

4. TURBULENT FLOW STRUCTURE IN THE SCOUR HOLE

The DES simulations are carried out in the scour hole region, assuming no-slip boundary conditions at solid walls. At the inlet we prescribe a converged URANS solution, previously computed in a separate calculation, which considers the entire length of the upstream rectangular channel and the geometry of the sluice gate. All the results presented in this investigation are obtained by using a non-dimensional physical time-step of $\Delta t = 0.005$. In this section we first show qualitatively the instantaneous resolved flow in the scour hole, and then we compute the instantaneous variables to reproduce the experimental observations reported by Albayrak et al. (2008).

To describe the instantaneous flow near the bed and elucidate the three-dimensional phenomena friven by the Görtler vortices, we visualize the coherent dynamics of the flow using the so-called q-criterion (Hunt, Wray, & Moin, 1988), defined as:

$$q = \frac{1}{2}\left(O_{ij}O_{ij} - S_{ij}S_{ij}\right) \tag{4.1}$$

where O_{ij} and S_{ij} denote the antisymmetric and symmetric part of the velocity gradient tensor respectively.

According to Hunt et al. (1988), we can identify vortical structures in regions where $q > 0$, where the local rotation rate dominates the strain rate.

Figure 4.1 shows a snapshot of q-isosurfaces colored with the instantaneous streamwise vorticity Γ_x. Results show the overall complexity of the flow at this state of advanced erosion. The simulations capture the coherent structures dynamics near the bed and resolve the dynamics of the Görtler vortices. Animations of q-isosurfaces showed that inside the scoured region the flow is dominated by the shear-layer produced by the wall-jet that emanates from the flat-bed channel, identified as V2 vortices in figure 4.1(a). These horizontal structures exhibit significantly smaller time-scales compared to the Görtler vortices. On the other hand, pairs of streamwise structures identified as V1 in figure 4.1(a) and figure

4.1(b) occupy a significant portion of the bed within the scour hole. They appear intermittenly and move laterally with low frequencies as reported by Albayrak et al. (2008). It is important to note that the centrifugal instability is naturally excited by the resolved flowfield inside the scoured region, and Görtler vortices appear without imposing an unsteady pseudo-turbulent inflow condition. In addition, to test the importance of wall roughness, we performed simulations (not shown herein) with the same inflow conditions and geometry of the channel assuming a smooth wall in the concave bed. The computation demonstrated that Görtler vortices also developed over a smooth wall indicating that surface roughness is not a prerequisite to trigger the instability in this flow.

The emergence of pairs of counter-rotating vortices can also be studied by plotting contours of streamwise vorticity (Ω_X). In figure 4.2(a) we can clearly observe the Görtler vortices in the plane $X/b = 7$, inside the scour hole. The instantaneous streamlines and vorticity countours plotted in the zoomed area in figure 4.2(b), show that the flowfield is drastically altered in the concave region of the bed. After the boundary layer reattaches in the scour hole, highly unsteady vortices emerged and form mushroom-like structures with converging lateral flow, and strong vertical flow away from the wall, a feature of Görtler vortices that has commonly been observed as reported in the literature (Saric, 1994; Tandiono et al., 2008).

The presence of different scales make this flow a great challenge to be simulated. Additionally to different time-scales visualized in simulations, is clear the presence of vortices with different spatial scales. The shear-layer in the scoured region generate a recirculation in high zone and reattached zone at the bed is shown in figure 4.3.

An important finding obtained from the DES computations is that the Görtler vortices develop in both directions from the reattachment point. The coherent structure dynamics from the simulations showed that pairs of longitudinal vortices are also formed in the upstream direction for $X/b < 7.2$, as is shown in figures 4.2, 4.3 and 4.4. Therefore after the wall-jet reattaches to the sand bed, Görtler vortices form in opposite directions inside the recirculation vortex near the wall, and on the upslope face to the dune.

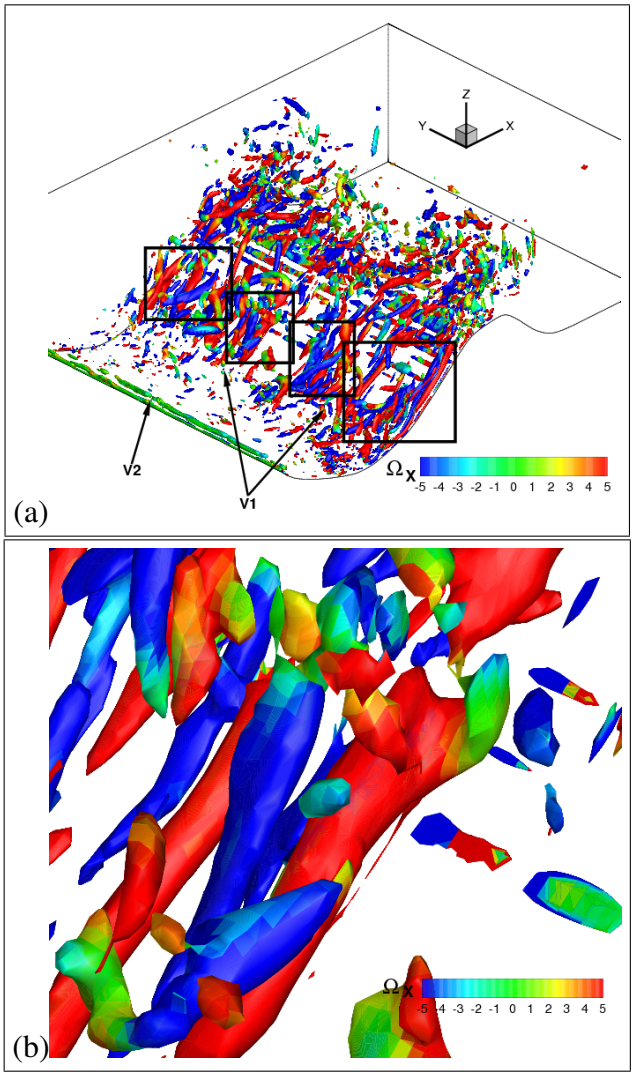

FIGURE 4.1. (a) Instantaneous 3D vortical structures on the concave bed visualized with q-isosurfaces. In red and blue color are vortices with positive and negative vorticity in streamwise X-direction. (b) Zoomed area inside the second rectangle, showing a detail of a pair of counter-rotating streamwise Görtler vortices in the scoured bed.

To simplify the analysis and evaluate if appropriate conditions exist for the development of the centrifugal instability in both directions, we plot the time-averaged velocity and test the inviscid criterion of Rayleigh for centrifugal instability at both sides of the reattachment point as shown in figure 4.5. Rayleigh circulation criterion for the circulation Γ can be written as follows (Saric, 1994):

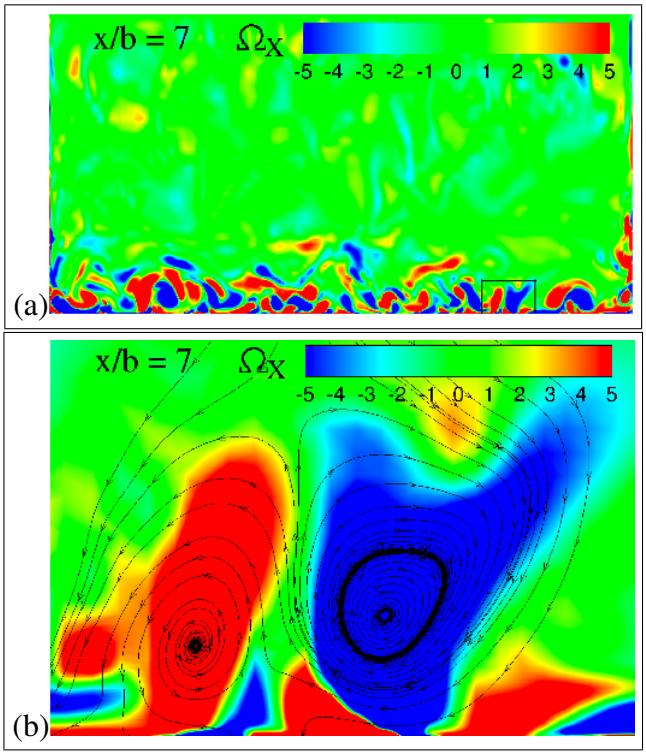

FIGURE 4.2. Contours of vorticity in x-direction. (a) Non-dimensional streamwise vorticity contours in the entire plane. (b) Zoomed area inside the rectangle with instantaneous streamlines shows clearly the counter-rotating vorticity and the mushroom structure generated by the vortex pair.

$$\frac{\partial \Gamma^2}{\partial r} < 0, \qquad \text{ANYWHERE IN THE FLOW} \tag{4.2}$$

where Γ is the circulation defined as $\Gamma = rV$. In this definition of a shear flow over a concave surface, r is the radius of curvature of the bed and V is the tangential velocity component. Rayleigh establishes that of $|rV|$ decreases with the radius r the flow is potencially unstable (Saric, 1994). As depicted in figure 4.5, these instability conditions are present in both sections. At the plane $X/b = 7.37$, downstream of the reattachment region, the time-averaged velocity profile does not have inflection points bu Rayleigh circulation criterion shows a potencial unstable profile. At plane $X/b = 6.16$, upstream from the reattachment, the velocity profile and Rayleigh criterion reveal the potential development of a

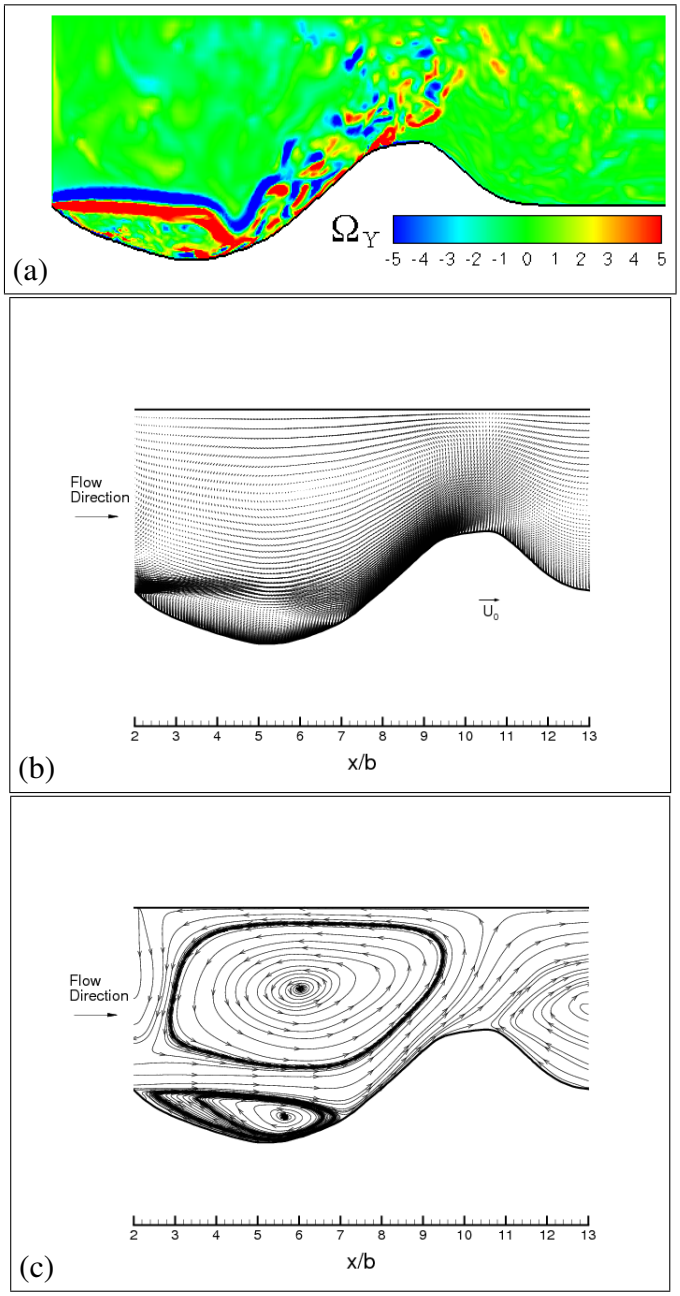

FIGURE 4.3. (a) Contours of non-dimensional vorticity in *y*-direction at center of the channel. (b) Velocity obtained with the mean flowfield at the center of the channel. (c) Streamlines at center of the channel shows the magnitude of flow scales. Is clear the reattached zone at the bed where appear Görtler vortices in opposite direction to the mean flow.

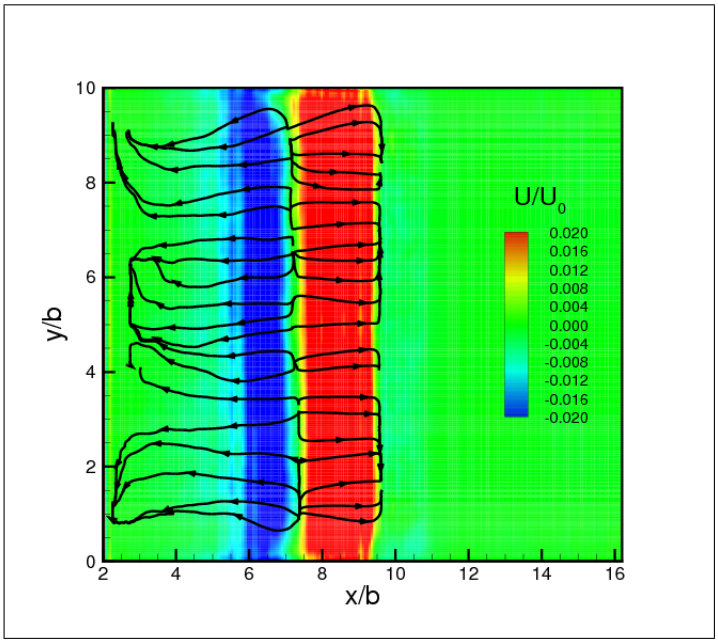

FIGURE 4.4. Two zones of positive (blue color) and negative (red color) average velocity at the bed are plotted. The reattachment point is located at X/b 7.2

centrifugal instability. These results point to the conclusion that there are favorable conditions for the development of the centrifugal instability in the upstream and downstream directions after the wall-jet reattaches to the sand bed, which is captured by the numerical simulations.

The manifestation and presence of counter-rotating streamwise Görtler vortices increases the levels of turbulent kinetic energy (TKE), which is defined as follows:

$$TKE = \frac{1}{2}\left(\langle u'^2\rangle + \langle v'^2\rangle + \langle w'^2\rangle\right) \tag{4.3}$$

where $\langle u'^2\rangle$, $\langle v'^2\rangle$ and $\langle w'^2\rangle$ are the time-average square velocity fluctuations.

Figure 4.6 shows the distribution of the resolved TKE at different planes in streamwise flow direction. In these figures is clear the increase of TKE by the presence of counter-rotating streamwise Görtler vortices. At first slices, figures 4.6 (a), (b) and (c) present lower values of TKE at the bed in comparison to the planes $x/b = 6$, $x/b = 7$ and $x/b = 8$ where

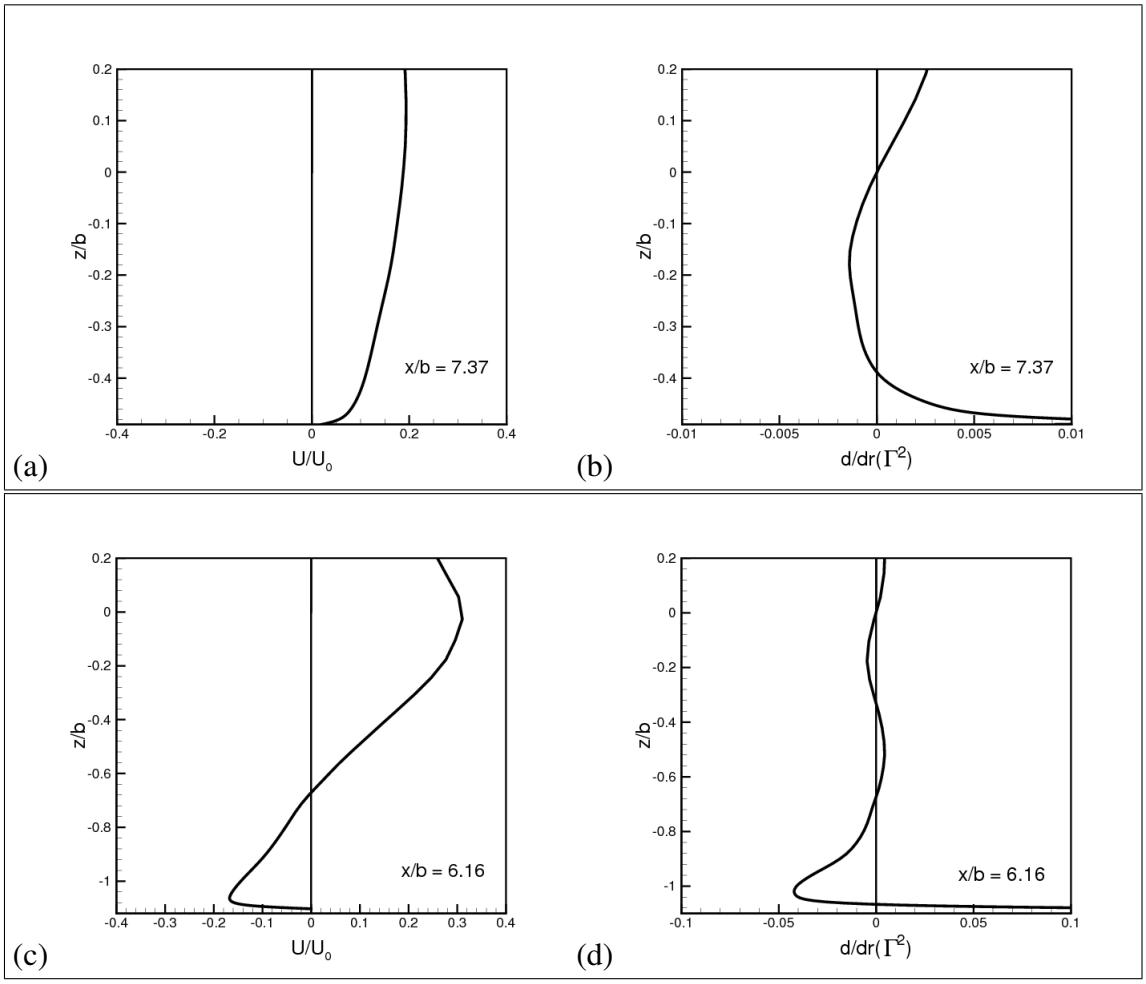

FIGURE 4.5. (a) Time-average velocity profile near he bed at plane $X/b = 7.37$; and (b) Rayleigh circulation criterion calculated at plane $X/b = 7.37$. (c) Time-average velocity profile near he bed at plane $X/b = 6.16$; and (d) Rayleigh circulation criterion computed at plane $X/b = 6.16$. In both cases the criterion reveal favorable conditions for the development of couter-rotating Görtler vortices in opposite directions, as seen in DES computations.

Görtler vortices are developed. At first planes is clear the high values of TKE produced by wall-jet shear-layer coming from sluice gate at $z/b = 0$, but in last slices the high values of TKE are present at the bed.

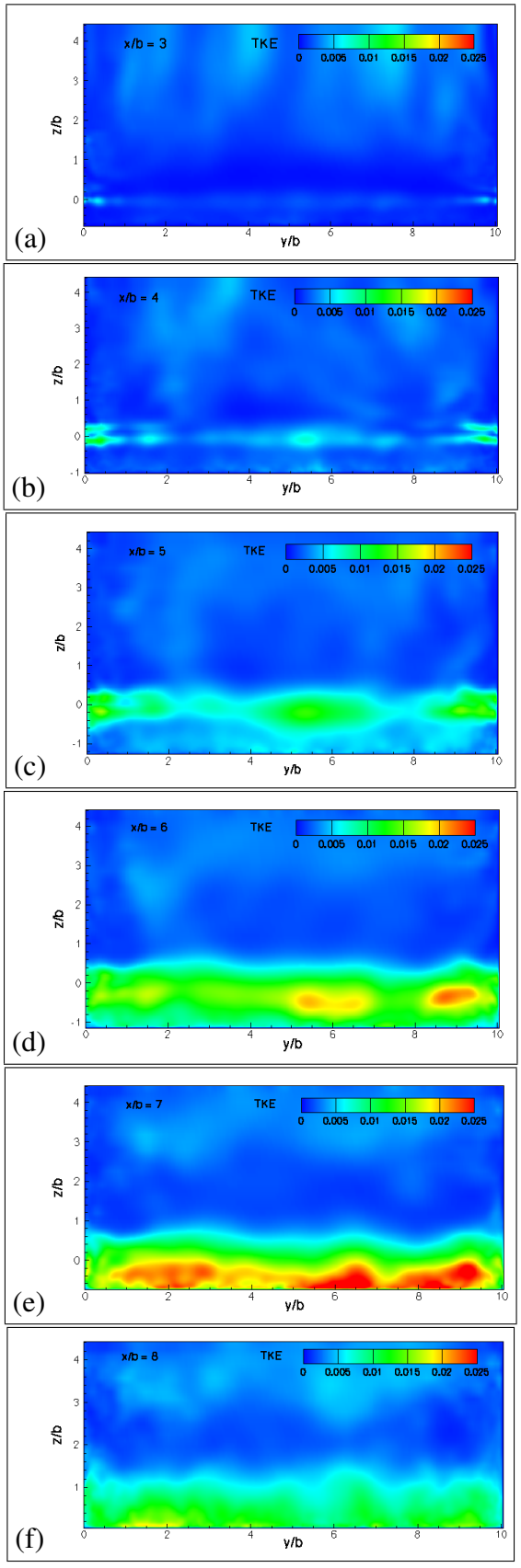

FIGURE 4.6. Turbulent kinetic energy at different planes in streamwise direction. (a) $x/b = 3$. (b) $x/b = 4$. (c) $x/b = 5$. (d) $x/b = 6$. (e) $x/b = 7$. (f) $x/b = 8$.

5. SHEAR STRESS AND STATISTICAL FLOW RESULTS

Our simulations show the turbulent Görtler vortices that are formed in the downstream section of the concave bed are dominated by low-frequency unsteadiness, and they are directly responsible for the increments on the instantaneous stresses on the bed. Figure 5.1(a) show the time series of the instantaneous non-dimensional shear velocity (u_τ) at the bed, at plane $x/b = 8$ inside the scour hole. In this figure is clear the presence of peaks with intermmitency, properly of the appearance of Görtler vortices which is in accordance with animations and results of (Albayrak et al., 2008). This peaks values reaches three times mean low values of shear velocity. Is important to note that these high values of non-dimensional shear velocity at different intervals of time are responsible for the initiation of particle motion visualized by Hopfinger et al. (2004) and Albayrak et al. (2008). Our model is capable to capture with a great detail this feature, which is impossible to visualize only with its averaged terms, as is shown in figures 5.1 (b) and (c).

In figure 5.1(b) we can observe an increase in the intensity of u_τ at zone where Görtler vortices are developed. This shows the spatial variation of instantaneous non-dimensional shear velocity, along the spanwise direction across the Görtler vortices. When these vortices are present, the shear-stress has a semingly periodic variation across the channel. This effect was reported by Hopfinger et al. (2004), as they observed considerable increments of sediment transport rates in this area of the bed.

High values of u_τ in figure 5.1 correspond to the positions of the streamwise vortices, while lower values are located in between them. This plot also has a remarkable similarity with the skin friction profiles reported in the recent experiments of (Tandiono et al., 2009), who measured the effects of Görtler vortices in the turbulent flow inside a curved rectangular duct.

The spatial variation of the shear-stress generated by the Görtler vortices is also responsible for the emergence of bed forms, identified as sediment streaks by (Hopfinger et al., 2004). Their experimental visualizations showed the appearance of streamwise oriented

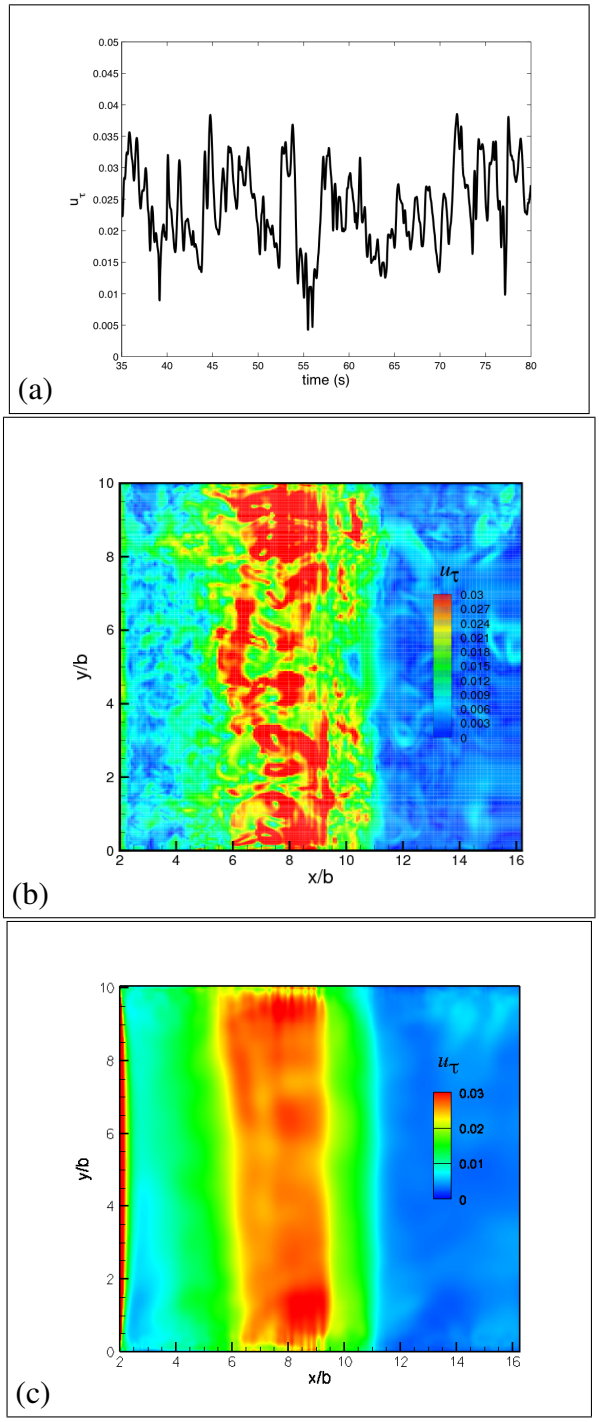

FIGURE 5.1. (a) Time-series of non-dimensional shear velocity at the center of the channel at the plane $X/b = 7.37$. (b) Instantaneous non-dimensional shear velocity at the bed. (c) Non-dimensional shear-velocity averaged on time-series data. There is a significant increase on the shear-velocity magnitude where Görtler vortices are developed.

streaks on the mobile bed, which were identified as evident signs of the presence of Görtler vortices and their effects on bed load transport and scouring processes.

In the streamwise direction we observe that the shear velocity presents higher magnitudes in the section comprised by $7 < x/b < 9$, at the center of the channel. This feature, attributed to the Görtler vortices and shown in figure 5.1, was also described in the experimental investigation of (Albayrak et al., 2008). With respect to this area of high stress, they make the following comment: *"This higher dimensionless friction velocity on the concave wall, when $x/b > 7$, can be attributed to the development of Görtler vortices. When $x/b > 9$, the friction velocity on the concave wall starts to decrease, because after that point the boundary slope changes and the Görtler vortices disappear."*

From our simulations we can reproduce additional quantitative results that were also obtained by Albayrak et al. (2008). Employing instantaneous measurements of the velocity field in a vertical profile, they compute the product of horizontal and vertical velocity fluctuations in time, capturing upwash and downwash flow events near the bed. These events are characterized by positive and negative values of the instantaneous components of the Reynolds stress tensor. Along a vertical line in the center of the channel, at a position $x/b = 7$, the flowfield is plotted in time. The vertical distance is non-dimensionalized by using the length scale $z'_{1/2}$ defined as the height at which the velocity magnitude is equal to half of the maximum streamwise velocity (Albayrak et al., 2008). Remarkably the simulations presented in this research can capture the same dynamics described by Albayrak et al. (2008). In figure 5.2(a) we plot the velocity components and contours of $u'w'$ in time, using the resolved flowfield from the DES calculation. This figure shows the predominant contribution of upwash events on the Reynolds stresses. In the outer layer, the downwash and upwash flow events are dominant at several locations, see for example $z'/z'_{1/2} = 1$ and $z'/z'_{1/2} = 0.5$ at $t = 8.9$ s and $t = 9.2$s The same statistical observations were made by Albayrak et al. (2008), who linked these dynamic processes to the unsteadiness of the near-wall coherent vortices. Convergent flow observed in plots of $v' - w'$ velocity vector which were reported by Albayrak et al. (2008), are also reproduced in our simulations as shown in figure 5.2(b).

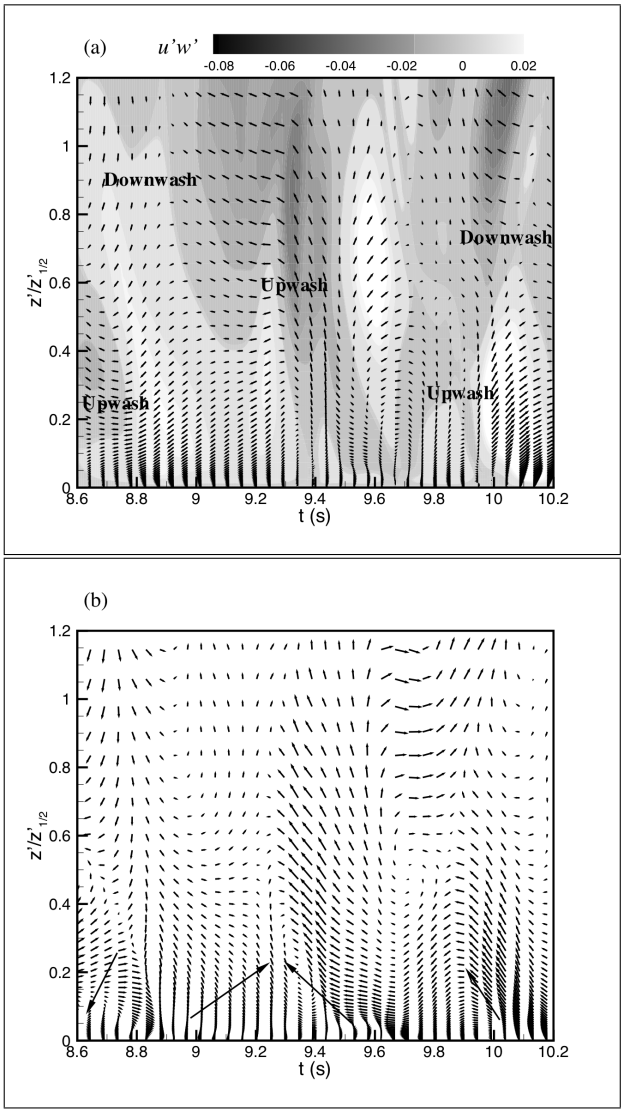

FIGURE 5.2. Two-dimensional resolved velocity vector plots along a vertical profile at plane $x/b = 7$, at the center of the channel. The total time interval is $\Delta t = 1.6s$. The length scale is $z_{1/2} = 5.8$ cm. on the selected profile. (a) Streamwise (x,z')-plane, velocity vectors ($u'w'$); (b) Spanwise (y,z')-plane, velocity vectors (v', w').

Another quantitative results that has a direct relation with the influence of Görtler vortices on scoured region is the Reynolds stress obtained from the resolved velocity fluctuations. Figure 5.3 shows the $\langle u'w' \rangle$ Reynolds stress computed by Albayrak et al. (2008) at plane $x/b = 6$ and the results obtained from our DES simulations. In this figure is clear that

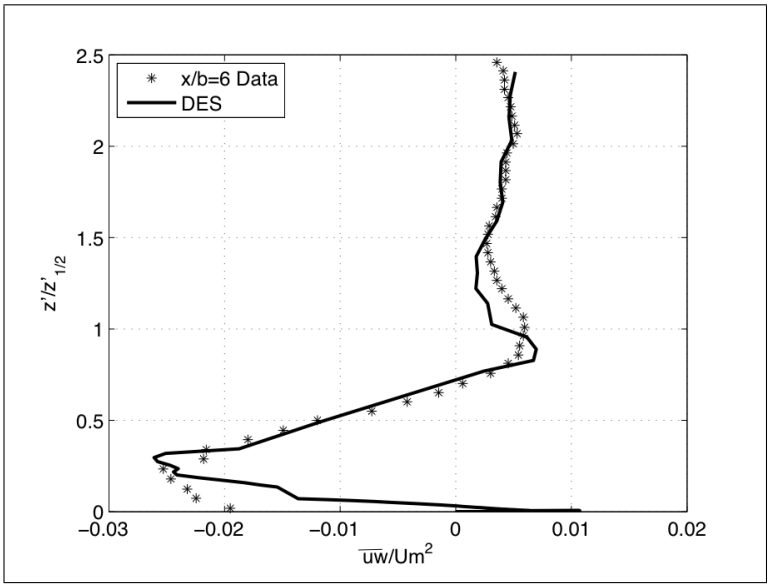

FIGURE 5.3. Dimensionless Normal Reynolds stress computed in experiments made by *Albayrak et al.* (2008) (*) and the DES model (-), at plane $X/b = 6$. The values of Reynolds stress are scaled by U_m, which correspond to the maximum streamwise average velocity.

DES can represent with a godd accuracy the experimental results measured by Albayrak et al. (2008).

In the same direction with statistical upwash and downwash events obtained with our model, we compute the autocorrelation of Dimensionless Normal Reynolds stresses ($u'w'/U_m$) at scoured zone where Görtler vortices are developed ($X/b = 7$), as is shown in figure 5.4. This figure established the presence of a periodic series of increments of shear stress at the bed. This is clear when dominant frequencies of *u,v,w* and Normal Reynolds shear stresses ($u'w'$) are calculated. The three largest dominante frequencies of these variables are in Table 5.1.

From calculated data in Table 5.1 is clear the presence of quasi-periodic series for the three velocity components, which manifest the appearance, developing and dissipation of Görtler vortices in the scoured region in a quasi-periodic process. Similar dominant frequencies in streamwise and vertical velocity components, suggest the presence of downwash and upwash events showed in figure 5.2(a) and reported in the experiments

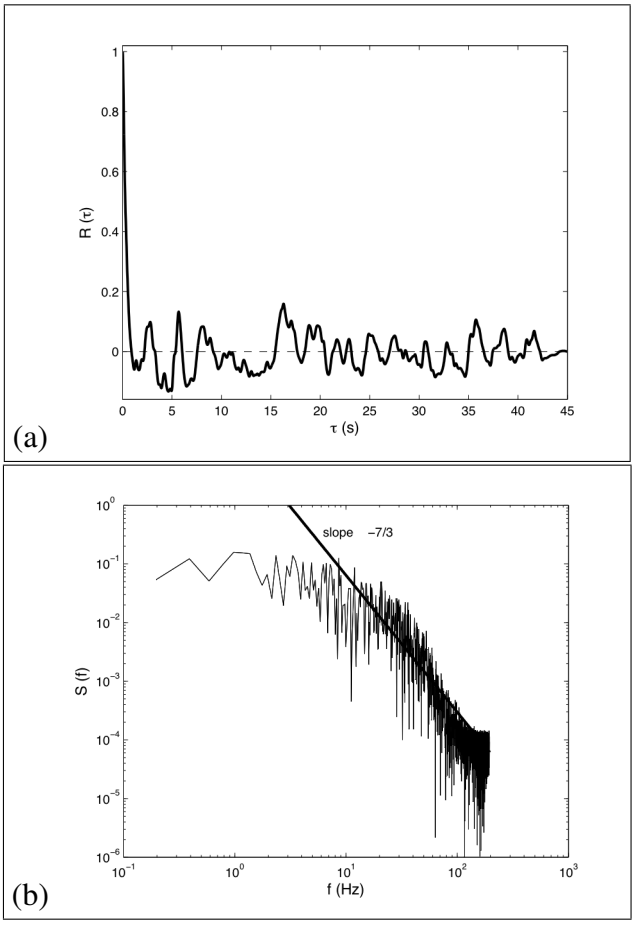

FIGURE 5.4. (a) Autocorrelation and (b) Frecuency spectrum of Normal Reynolds shear stress time series at the bed at $x/b = 7$ and at the center of the channel, where Görtler vortices are developed.

of Albayrak et al. (2008). In figure 5.4(b) is shown the Reynolds shear stress frequency spectrum, which follows a power-law of -$7/3$ as is suggested by Pope (2000).

TABLE 5.1. Dominant frequencies of three velocity components and Normal Reynolds Stress

Variable	Frequency 1 (Hz)	Frequency 2 (Hz)	Frequency 3 (Hz)
u	0.39	0.78	1.56
v	0.20	0.59	1.17
w	0.39	0.78	1.56
u'w'	0.39	0.98	2.35

6. SEDIMENT TRANSPORT MODEL

The numerical simulations performed for the flow downstream of a sluice gate reproduce the experimentally observed flow physics reported by Hopfinger et al. (2004) and Albayrak et al. (2008). A properly designed sediment transport model can take advantage of the instantaneous information of the coherent structures of the flow to investigate the sediment dynamics at erosion zone in clear-water scour conditions. As it was mentioned previously, counter-rotating Görtler vortices dynamics are responsible for enhancing the shear stresses at the bed, increasing the magnitude of sediment transport rates and producing bed forms as streaks (Hopfinger et al., 2004; Albayrak et al., 2008). This interaction between Görtler vortices and sediment transport motivates the use of a sediment transport model that can make use of the flowfield provided by the DES simulations.

In this chapter, we review the concepts behind the development of models for multiphase flows in pratical applications and establish the rationale for using a Lagrangian particle model of sediment transport in the flowfield downstream of a sluice gate at the erosion zone studied previously. The governing equations and methods to integrate the trajectory and momentum of particles located at the scour region for the computed flowfield are then presented. From the results of simulations we can investigate further the effects of the unsteady coherent structures near the bed (especially Görtler vortices), and the entrainment and deposition processes that occur in bed-load transport. The results of these simulations shows qualitatively the representation of the advanced scoured bed zone, but provide insights to comprehend the effects of Görtler vortices on scour process and sediment streaks reported by Hopfinger et al. (2004).

6.1. Modeling of multiphase turbulent flows

The approaches developed to model multiphase flows in high Reynolds number turbulent flows can be generally classified as Eulerian (continuum) models, or Lagrangian models (Escauriaza, 2008; Escauriaza & Sotiropoulos, 2011a, 2011b).

Eulerian models have been employed for the prediction of interpenetrating media and particle flows, considering the particles (or dispersed phase) as a continuum fluid (Crowe et al., 1998). The simplest *one-fluid* approach consists on solving an equation for the conservation of mass of the particles, determining the mean spatial concentration from an advection-diffusion relation. The governing equations can be modified in cases when the phases exhibit considerably density differences or the particle flux includes a vertical term to model the effects of gravity (Escauriaza & Sotiropoulos, 2011a, 2011b). A more complete Eulerian approach can be developed by considering the particle phase as another fluid. In the so-called *two-fluid* approach, the dynamics of the carrier fluid and the particles are computed by solving separate conservation of mass and momentum equations for each phase (Drew, 1983). The equations are coupled by force terms that model the exchange of momentum between the particles and the fluid, which is called *two-way* coupling as explained below. These Eulerian models also need to incorporate models for the turbulent terms that appear after averaging the equations, since correlations of fluctuating quantities have to be closed to represent the unresolved concentration and velocity fields (Lakehal, 2002). Conventional Eulerian models have been applied to sediment transport problems, usually based on one-equation models to compute the sediment concentration. They have been shown to reproduce the suspended load in practical applications at high-Reynolds numbers flows (e.g. Wu et al. (2000)) but the approximations implied in an advection-diffusion equation for sediment concentration can generate inconsistent fluxes near the bed in 3D unsteady flows, where the interaction with the wall and the flow produce a complex dynamics of the sediment (Chang & Scotti, 2004).

Lagrangian models for multiphase flows consider the dynamics of individual particles whose motion is controlled by advection mechanisms generated by the continuum surrounding Newtonian fluid, interactions with other particles and the gravitational force (Loth, 2000). Depending on the particle concentration, flows should be treated differently in order to consider the relevant mechanisms that drive their dynamics. Dense flows with high concentrations of particles are mainly controlled by particle-particle collisions and by the changes on the flowfield produced by fluid-particle interactions. In dilute flows, on the

other hand, concentrations are low and interparticle collisions have a very small influence on the particle dynamics compared to the effects of the flowfield (Crowe et al., 1996).

As pointed out by Crowe et al. (1996), no flow is completely dilute or dense and modeling techniques should be able to describe the relevant physics in each specific case. Fully resolved simulations of particles in turbulent flows (particle DNS) cannot be applied due to their computational costs, since they require to solve the flowfield at the particle surface in detail. A resolved representation of particles in a fluid flow is also clearly limited by its range of applicability, restricting its application to theoretical investigations for low-Reynolds numbers and simple geometries (see for instance the simulations of Burton and Eaton (2005) for a single fixed paricle in decaying isotropic turbulence in a box). Therefore, point-volume formulations are the only feasible approach to describe the dynamics of multiple particles in practical situations (Loth, 2000). The point-volume model utilize the particle center of gravity to represent the position and trajectory of each particle, and analytical formulas are employed to reproduce the surface-averaged forces based on experimental results or theoretical approximations of the momentum transfer from the fluid to the particles or vice versa (see Maxey and Riley (1983); Crowe et al. (1998); Loth (2000); Michaelides (2003)).

Depending on the effects of the particles on the fluid flow, Lagrangian models of multiphase flows can be classified as *one-way coupling* or *two-way coupling* approaches (Crowe et al., 1996). A one-way coupling model assumes that the presence of particles does not have a significant effect on the flow dynamics, producing negligible local modifications of the flowfield or changes on the dynamics of nearby particles, which is tipically valid for dilute flows. Two-way coupling Lagrangian models, on the other hand, incorporate the effects of the particles on the flowfield adding a term to the Navier-Stokes equations to consider the forces exerted by the particles on the carrier fluid. For the computations of particle-laden turbulent flows, two-way coupling models have been proposed in the context of LES simulations (e.g. Maxey et al. (1997); Boivin et al. (2000); Hu and Celik (2008)). However, two-way coupled simulations of complex turbulent flows with multiple particles are still very limited to simple problems, since the calculation of the coupling terms with the

particle forces require the interpolation and distribution of particle stresses back to the grid nodes of the flowfield computation in the Eulerian framework (see Hu and Celik (2008), for example). The turbulence closure for URANS simulations or the subgrid SGS model of LES may also require additional modifications, depending on the influence of the particle flow on the unresolved scales of motion (Nadaoka et al., 1999; Lakehal, 2002).

Lagrangian models of sediment particles have been developed to study bed-load transport carried out with different degrees of detail. Initial studies only considered mean steady flows to develop theoretical models of particle saltation, initiation of motion, and bed-load transport models (Bagnold, 1973; Wiberg & Smith, 1985; Niño et al., 2002). Recently, Lagrangian models have also been developed to predict the trajectories of sediment particles over bed-forms in LES simulations (Chang & Scotti, 2003, 2006) and to investigate the initial stages of erosion and the development of ripples produced by the turbulent horseshoe vortex (THV) system in the vecinity of a surface-mounted cylinder (Escauriaza & Sotiropoulos, 2011a).

In present section we summarize the particle model of sediment transport used to investigate the effects of counter-rotating Görtler vortices on the generation of sediment streaks reported experimentally by Hopfinger et al. (2004) and Albayrak et al. (2008), with a diameter equal to the median diameter utilized in experiments ($d_{50} = 2$ mm). For more details of the model the reader is referred to the studies of Escauriaza (2008); Escauriaza and Sotiropoulos (2011a, 2011b), since this chapter just explain in the principal concepts and formulas employed in the simulations. This theoretical Lagrangian approach is a more complete and precise method to simulate the sediment motion produced by the forces generated by coherent structures. It is important to recognize, however, that tracking a large numbers of particles that participate in sediment transport phenomena in these complex engineering flows is computationally very expensive and impractical. Therefore, the Lagrangian model is not intended as means to predict scour downstream of a sluice gate because the large number of particles required to do that would make the simulation impractical. The model instead is meant to give fundamental insights into the initiation of

motion and the characteristics of the bed-load flux so that it can guide the development of continuum, macro-scale based models of bed-load transport.

The model of particle transport is a one-way coupling approach, since the sediment corresponds to fine sand with a diameter much a smaller than the well-resolved unsteady vortical structures studied in the previous chapter, which constitute the major sediment transport mechanisms for this problem. The flowfield simulation on the scour hole and the clear-water scour conditions of the flow determine that most of the dynamics will be represented by the resolved flowfield that is utilized to compute the particle dynamics.

By adopting this physically-based Lagrangian model, which considers the instantaneous forces exerted by the fluid in the motion of individual sediment grains, we seek to improve the representation of near-bed transport processes and have a better description of the characteristics of the unsteady bed-load transport by coherent-structures. The sediment transport is therefore studied by simulating the trajectory and momentum of individual sediment grains driven by the resolved flow on the scour hole.

To study the effects of Görtler vortices on the particle dynamics, we select a fixed area on the scour-hole, where Görtler vortices studied in the previous chapter develops. The particles have an initial zero velocity, and their forces are computed from the flowfield obtained from DES simulations. The model is not capable of giving insights into the erosion process but it provides an excellent tool for understanding the particle transport by large-scale unsteady vortical structures. Furthermore, we not model the erosion process from flat mobile bed to quasi-equilibrium erosion stage before Görtler vortices appear, but we model the effects of Görtler vortices at an advanced scour stage according to the experiences of Albayrak et al. (2008).

The details of the model, the calculation of the particle dynamics, and the investigation of the qualitative particle flux are studied in the next sections.

6.2. Governing equations and numerical calculation

The main challenge in simulating solid inertial particles in turbulent flows arises from the description of the forces utilized to derive the particle momentum equation. Therefore, the derivation of the governing equations should consider theoretical formulas for the forces that represent the most important features of transport, similar to the formulation developed in the landmark study of Maxey and Riley (1983) for spherical particles in non-uniform low-Reynolds number flows. Based on these formulations, simple models of forces have been developed for turbulent flows under different conditions (see for example Loth (2000); Michaelides (2003)), that have also been applied to sediment transport problems (e.g. Chang and Scotti (2003, 2006)).

As explained in the previous section, in the present case of clear-water scour with all the transport occuring as bed-load, we simplify the particle model for the sediment as a dispersed phase assuming that the instantaneous concentration of particles is always low, such that transport is considered dilute at all times. The governing equations describe the trajectory and momentum of a grain with a mass *m* by the following system of equations:

$$\frac{dx_i}{dt} = v_i \tag{6.1}$$

$$m\frac{v_i}{dt} = f_i \tag{6.2}$$

where v_i and x_i are the velocity and the position of the particle in each coordinate direction respectively, and f_i represents the sum of forces acting over the particle in the *i* direction.

The trajectory and momentum equations 6.1 and 6.2, describe the particle with a point-volume representation such that all the forces are concentrated on a point that corresponds to its center of mass and the continuum background fluid is not affeted by the particle motion. These are called *one-way coupling* simulations, since the solid phase does not alter the dynamics of the fluid (Escauriaza, 2008; Escauriaza & Sotiropoulos, 2011a, 2011b).

The hypotheses and formulas developed to represent the instantaneous forces exerted on the solid phase by the fluid are included in the model and presented in this section to

show the Lagrangian methodology for sediment computations. The model provides a more detailed description of the particle dynamics and accounts directly for the instantaneous resolved flow in the sediment transport dynamics.

6.2.1. Forces on sediment particles

The total force acting over the sediment particles, f_i in equation 6.2 , is generally composed of three differents parts:

- Gravitational or other body forces.
- Surface forces exerted by the fluid, such as drag or lift.
- Forces due to interaction with other particles, collisions with the bed, or another physical boundary within the flow.

These forces represent the transfer of momentum between the two phases, which controls the complex real-life motion of water and sediment grains. The following list provides a review of the forces and assumptions considered in the model:

a. Drag force: Drag is one of the dominant forces acting on the sediment particles, and its direction and total magnitude can be expressed by the well known semi-empirical relation obtained from dimensional analysis in steady uniform flows (Escauriaza, 2008; Escauriaza & Sotiropoulos, 2011a):

$$\mathbf{F}_D = \frac{1}{2}\rho C_D A|\mathbf{u}-\mathbf{v}|\left(\mathbf{u}-\mathbf{v}\right) \tag{6.3}$$

where *A* is a representative area of the particle, $\mathbf{u}$ and $\mathbf{v}$ are the fluid and particle velocities respectively, and ρ is the density of water. To determine the effect of viscosity on the total drag force exerted over the sediment grain we employ a drag coefficient, C_D, which is a function of the Reynolds number of the particle, scaled with the particle diameter and the relative velocity $\mathbf{v}_r = \mathbf{u} - \mathbf{v}$:

$$Re_r = \frac{|\mathbf{v}_r|d}{\nu} \tag{6.4}$$

There have been numerous studies addresing te estimation of the drag coefficient as a function of Re_r from experimental and theoretical analyses. By simplifying the Navier-Stokes equations in spherical coordinates for $Re_r < 1$, we can find an analytical solution for the drag coefficient within the so-called Stokes flow regime: $C_D = 24/Re_r$. For larger Reynolds numbers different relations have been determined for uniform flows in steady conditions and corrections have been proposed for non-uniform velocity fields (Crowe et al., 1998). In this research, the relation determined specifically for sand and gravel by Engelund and Hansen (1967) for $Re_r < 10^4$ is considered to model the drag force:

$$C_D = \frac{24}{Re_r} + 1.5 \tag{6.5}$$

b. Gravity Force: Gravity is the driving force controlling sediment entrainment and deposition. The total force is decomposed as the sum of the particle weight and the bouyancy force produced by hydrostatic vertical pressure gradient, which can be written as:

$$\mathbf{F}_G = \left(1 - \frac{1}{SG}\right) m\mathbf{g} \tag{6.6}$$

where $\mathbf{g} = -g\delta_{i3}$ is the acceleration of gravity, δ_{ij} is the Kronecker's delta utilized in the gravity term that acts on the negative x_3 direction, and $SG = \rho_s/\rho$ the sediment specific gravity.

c. Lift Force: The lift mechanism is a consequence of the velocity gradient and viscous shear stresses that induce a non-uniform pressure distribution over the particle. The basic relation for inviscid flows was developed by Auton (1987) and Auton et al. (1988), considering the velocity gradient around a particle moving in a non-uniform rotational flow. The lift force was derived as a function of the flow vorticity and the particle relative velocity, with a lift coefficient $C_L = 0.5$:

$$\mathbf{F}_L^{(1)} = \rho C_L \frac{\pi d^3}{6} \left(\mathbf{v}_r \times \omega\right) \tag{6.7}$$

where $\mathbf{v}_r$ is the relative particle velocity, and ω is the vorticity of the flow. In sediment transport applications, Parker et al. (2003) used this relation in the development of a bed-load transport model. Wiberg and Smith (1985) and Chang and Scotti (2006) used a linearized version of equation (6.7) to determine the magnitude of the lift force for spheres in initiation of motion analysis, particle saltation, and trajectories in an oscillating flow at the turbulent boundary layer.

For viscous flows, Saffman (1965, 1968) formulated an expression for lift at low Reynolds numbers computing the force perpendicular to the relative velocity field as a function of the viscosity, the fluid density, and the vorticity (or velocity gradient) at the particle position. Saffman's expression reads as follows:

$$\mathbf{F}_L^{(2)} = \rho 1.615 \frac{d^2 \nu^{1/2}}{|\omega|^{1/2}} \left(\mathbf{v}_r \times \omega\right) \tag{6.8}$$

For higher Reynolds number flows, Mei (1992) adapted Saffman's formula and derived an empirical relation depending on Re_r:

$$\begin{aligned} \mathbf{F}_L^{(3)} &= \mathbf{F}_L^{(2)} \left(1 - 0.3314\beta^{1/2}\right) \exp\left(\frac{Re_r}{10}\right) + 0.3314\beta^{1/2}, Re_r \leq 40 \\ &= \mathbf{F}_L^{(2)} 0.0524 \left(\beta Re_r\right)^{1/2}, \qquad\qquad Re_r > 40 \end{aligned} \tag{6.9}$$

where the variable β is defined as:

$$\beta = \frac{d}{2} \frac{|\omega|}{\mathbf{v}_r}, \qquad 0.005 < \beta < 0.4$$

In the present model, the equation for the particle momentum incorporates equation (6.9) to estimate the lift on fine sand grains, assumed to be non-rotating spheres, yielding an expression for the lift coefficient that is a function of the local vorticity magnitude and the particle Reynolds number, $C_L(|\omega|, Re_r)$. When the value of the parameter β that appears in equation (6.9) is outside the range of validity ($0.005 < \beta < 0.4$), we utilize Auton's relation with a constant value for C_L in equation (6.7).

d. Added Mass: The added mass effect is the force produced by the acceleration of fluid due the particle motion, which alters the surface stress distribution. For an inviscid and incompressible flow Auton et al. (1988) and Crowe et al. (1998) demonstrated that the virtual or added mass force acting on a sphere is:

$$\mathbf{F}_{AM} = \rho C_m \frac{\pi d^3}{6} \left(\frac{D\mathbf{u}}{Dt} - \frac{d\mathbf{v}}{dt} \right) \tag{6.10}$$

Assuming particles with spherical shape, the added mass force is then equivalent to the fluid momentum with half the volume of the particle, thus the added mass coefficient C_m can be assumed to be 0.5.

e. Interaction with the Bed: There are two types of bed-particle interactions accounted for in the present model. The first interaction involves the collision of sediment grains with the bed or solid boundaries of the computational domain, during which the normal and tangential momentum of a moving particle with respect to the surface are modified upon impact. The second interaction involves contact friction forces that resist the initiation of motion for a particle resting at the bed. To represent the collisions of sediment grains against the bed, an impact scheme with empirical coefficients with glass spheres and sediment particles of arbitrary shape that for fine sand the collisions are inelastic and produce no normal rebound since the momentum is damped by the intersticial fluid. When a moving particle collides with the bed, its trajectory and momentum are modified by eliminating the normal component to the surface, and reducing the tangential momentum by a factor of 0.9, following the recommendations of Schmeeckle et al. (2001). On the other hand, a Couloumb force is considered to account for frictional resistance when particles are resting at the bed surface. The direction of the force is taken as the opposite of the local bed-tangent instantaneous resultant force of the body and surface forces, and its magnitude is proportional to the particle force projected in the normal direction of the bed (Bagnold, 1956):

$$\mathbf{F}_S = -\mu_S \left(\mathbf{F} \cdot \hat{n}\right) \frac{\mathbf{F} - \left(\mathbf{F} \cdot \hat{n}\right) \hat{n}}{\left|\mathbf{F} - \left(\mathbf{F} \cdot \hat{n}\right) \hat{n}\right|} \tag{6.11}$$

where $\mathbf{F}$ is the local force acting on the particle, $\mu_S = 0.62$ is the static friction coefficient, and $\hat{n}$ the normal vector to the bed surface (Bagnold, 1956).

Additional forces that could become important in determining the particle dynamics arise due to the so-called Basset or history effect and particle-to-particle interactions. The Basset or history term is neglected in the model used in this work. Additional difficulties have also arisen from its definition in high Reynolds number turbulent flows (see the comments made by Chang and Scotti (2003)). Collisions among particles are also neglected since the sediment concentration is assumed to be low at all times.

The momentum equation for a single particle, equation (6.2), can now be written in terms of the modeled forces described above. The Lagrangian particle model will provide a more detailed representation of sediment transport, using the resolved flowfield from the DES computations to evaluate the deterministic transport by large-scale coherent structures.

6.2.2. Particle momentum equation in non-dimensional form

Considering all the forces described in the previous section, the complete momentum equation is obtained by adding the forces on the right-hand side of equation (6.2). As discussed by Loth (2000), however, the simple addition of the forces may not be correct due to non-linear interactions among all the fluid forces, but generally these effects are assumed to be small and can be neglected.

The forces described in the previous section that are included in our Lagrangian model of sediment transport arise from the perturbations induced by the particle presence in the fluid flow. Maxey and Riley (1983) and Auton et al. (1988) demonstrated that in the derivation of the complete momentum equation for a particle the effect of the undisturbed fluid stresses also appears on the balance of forces. The stresses produced by the undisturbed flowfield at the particle location correspond exactly to the forces that would exist in the

absence of the particle, which are produced by the acceleration of the displaced fluid mass (for the detailed derivation and discussion the reader is referred to the studies of Maxey and Riley (1983); Auton et al. (1988)).

Therefore, the momentum equation utilized in the model used for these simulations, for small non-rotating particles (fine sand) in dilute conditions can be expressed in vectorial form with dimensional quatities as follows,

$$\begin{aligned} m\frac{d\mathbf{v}}{dt} &= \frac{1}{2}\rho C_D A|\mathbf{v}_r|\mathbf{v}_r + \left(1-\frac{1}{SG}\right)m\mathbf{g} + \rho C_L \frac{\pi d^3}{6}\left(\mathbf{v}_r \times \omega\right) \\ &\quad +\rho C_m \frac{\pi d^3}{6}\left(\frac{D\mathbf{u}}{Dt} - \frac{d\mathbf{v}}{dt}\right) + \rho\frac{\pi d^3}{6}\frac{D\mathbf{u}}{Dt} \end{aligned}$$

which includes the expressions for drag, gravity, lift, added mass, and fluid stresses (Loth, 2000), and it should also consider the force expressed in equation (6.11) in case the particle is lying at repose on the bed. For out bed collision model, when a moving particle is located at a distance $d/2$ from any solid boundary the component of the momentum normal to the boundary surface is eliminated while the tangential component is reduced by a factor of 0.9 (Schmeeckle et al., 2001). The model that arises from all these considerations is very similar to the Lagrangian particle model of sediment grains utilized by Chang and Scotti (2003, 2006), except for the inclusion of the particle-bed interaction, and the complete non-linear form of the lift force used in the present model, in which the coefficient C_L depends on the flowfield and the particle diameter.

To simplify equation (6.12) we consider forces per unit mass by dividing the entire equation by the particle mass $m = \rho_s \frac{\pi d^3}{6}$. The resulting equation can be non-dimensionalized by utilizing the same velocity and length scales of the flow, $\mathcal{U}$ and $\mathcal{L}$ respectively, where $\mathcal{L}$ is equal to the water depth inmediately downstream sluice gate $h_2 = 0.22$ m. The momentum equation (6.12) can then be written in tensor notation, using also the expression for the particle specific gravity $SG = \rho_s/\rho$, in the following non-dimensionalized expression:

$$\frac{dv_i}{dt} = \frac{1}{SG}\frac{3}{4}\frac{C_D}{d}|\mathbf{v}_r|v_{ri} + \frac{1}{SG}\frac{\mathcal{L}}{\mathcal{U}^2}(SG-1)(-g\delta_{i3}) + \frac{1}{SG}C_L(\epsilon ijk v_{rj}\omega_k) + \frac{1}{SG}(1+C_m)\frac{Du_i}{Dt} - \frac{C_m}{SG}\frac{dv_i}{dt}$$

where the relative velocity is defined as $v_{ri} = u_i - v_i$ and ϵ_{ijk} is the tensorial permutation symbol to determine the vector perpendicular to the relative velocity and vorticity fields in the lift term.

The final non-dimensionalized form of the particle governing equations is expressed in terms of non-dimensional parameters that will be subsequently discussed, as follows:

$$\frac{dv_i}{dt} = \frac{1}{(SG+C_m)}\left[\frac{1}{St}v_{ri} - \frac{\delta_{i3}}{Fr^2} + C_L\left(\epsilon_{ijk}v_{rj}\omega_k\right) + (1+C_m)\frac{Du_i}{Dt}\right] \tag{6.12}$$

where *St* and *Fr* are known as the Stokes and Froude numbers respectively, and $SG = 2.65$ is the sediment constant specific gravity. This equation can be easily adapted for particles in contact with the bed, adding a tangential force to the surface that is computed as proportional to the normal component of the right hand side of the momentum equation (see also (6.11)).

In the present Lagrangian model of sediment transport used in these simulations, a series of dimensionless parameters can be readily identified in the particle momentum equation (6.12). Considering the drag force to be one of the leading forces exerted by the flow on a spherical particle, equation (6.3), we can identify a non-dimensional parameter based on the relative velocity, the particle diameter, and the Reynolds number of the flow. Namely, the ratio between the particle response time determined from the drag force on the particle and the characteristic time-scale of the flow. This parameter describes the dynamics of the dispersed phase and is known as the Stokes number, which can be expressed as follows (Escauriaza & Sotiropoulos, 2011a, 2011b):

$$St = \frac{4}{3}\frac{d}{C_D|\mathbf{v}_r|} \tag{6.13}$$

where the relative velocity magnitude $|\mathbf{v}_r|$, and particle diameter *d* are non-dimensionalized by the characteristic velocity and length-scale of the flow. From the Stokes number we can identify the dynamic relation between the two phases as follows: For $St \ll 1$ the particles have enough time to respond to changes in flow velocity and they can follow closely the motion of the largest scales of the flow. On the other hand, if $St \gg 1$ the particle velocity is less affected by the flowfield (Crowe et al., 1998). For the present simulation the size of sediment grains corresponds to a non-dimensional particle diameter $d = 0.009$, which yields $St \ll 1$. Consequently, we anticipate that in the simulations we will report below, the energetic large-scale flow structures will have a significant role on transport.

The other non-dimensional parameter that appears in the gravity term of equation (6.12) is the Froude number, *Fr*, defined as follows:

$$Fr = \frac{\mathcal{U}}{\sqrt{(SG-1)g\mathcal{L}}} \tag{6.14}$$

The Froude number relates the inertial and gravity forces of the particle-fluid system, and can characterize the relative effect of the gravitational term in the momentum equation.

With the trajectory and momentum equations defined from the derivation of the relevant forces acting on the particles, the particle position and velocity are obtained by integrating numerically the governing equations. The model is based on the vectorial approach of Kovacs and Parker (1994) and Parker et al. (2003) for determining the bed-load flux coupled with a new equation for calculating the instantaneous bed-load layer. The sediment flux vector, which is used as input of the Exner equation solved to determine the instantaneous bed elevation (see equation (6.19) below), is computed as the volume rate of sediment integrated within the bed-load layer, and is calculated as the product between the bed-areal concentration γ, which indicated the sediment volume per unit of area that contributes to transport, and the sediment velocity vector in the bed-load layer. The equation of the bed-load flux can thus be written in tensor notation $(j = 1, 2)$, as follows:

$$q^j = \gamma V^j \tag{6.15}$$

The key idea of the model is compute the sediment velocity in the bed-load layer by solving the momentum equation of the particles, equation (6.12) (Escauriaza & Sotiropoulos, 2011a), but transformed to the Eulerian framework attached to the bed and considering intantaneous forces computed from the resolved DES flowfield. For the expressions used to compute the sediment velocity see Escauriaza and Sotiropoulos (2011a). To compute the bed-areal concentration is used a formula from the relation for the percentage of moving particles per unit area of Engelund and Fredsøe (1976), which was also employed in the scour simulations of Roulund et al. (2005). Engelund and Fredsøe (1976) introduced an expression for the probability of a particle moving on the bed p_{ef} computed as function of the shear-stress as follows,

$$p_{ef} = \left[1 + \left(\frac{\pi\mu_d/6}{\tau_* - \tau_{*c}}\right)^4\right]^{-1/4} \tag{6.16}$$

where μ_d is the dynamic friction coefficient, τ_* the non-dimensional shear-stress or Shields number, and for the critical non-dimensional shear-stress τ_{*c}, is used the correction used by Roulund et al. (2005) in beds with arbitrary slope, which is expressed as follows,

$$\tau_{*c} = \tau_{*c0}\left[\cos\beta\left(1 - \frac{\sin^2\alpha\tan^2\beta}{\mu_s^2}\right)^{1/2} - \frac{\cos\alpha\sin\beta}{\mu_s}\right] \tag{6.17}$$

where τ_{*c0} is the critical Shields parameter for horizontal beds, μ_s is the static friction coefficient, α is the angle between the local flow velocity and the direction of maximum steepnes, and β is the angle of local bed inclination with respect to a horizontal plane (Roulund et al., 2005).

Assuming that the fine sand particles can be represented by spheres, it is computed the areal concentration γ using p_{ef} and the number of particles per unit area. Then, the final expression for γ is

$$\gamma = \frac{1}{6}\pi d^3 \frac{p_{ef}}{d^2} \tag{6.18}$$

Finally, to determine the instantaneous bed elevation, the sediment mass balance at the bed or Exner equation is employed, whose generalized form has been given by Paola and Voller (2005). In curvilinear coordinates, the Exner equation is expressed as follows,

$$\frac{\partial b}{\partial t} = \frac{-1}{(1-\lambda_p)} \left[\frac{\partial \gamma}{\partial t} + J \frac{\partial}{\partial \xi^j} \left(\frac{q^j}{J} \right) \right] \tag{6.19}$$

where b is the bed elevation, λ is the porosity that is assumed as constant and equal to 0.35, γ is calculated from equation (6.18), and the bed-load flux is calculated from equation (6.15). These are the principal equations and ideas about sediment transport model.

Escauriaza and Sotiropoulos (2011b) carried out simulations of particles located in the region influenced by the unsteadiness of the THV system by placing up to 10^5 sediment grains at repose on top of the flat bed in front of a cylinder. The simulations showed that the interaction of the vortices with the wall is the fundamental mechanism that increases the instantaneous bed shear-stress and produces transport. From the numerical results of the Lagrangian simulations, Escauriaza and Sotiropoulos (2009) also quantified and characterized the statistics of the bed-load flux by studying the time-series of transport behind a cylinder.

With this model we can investigate qualitatively the influence of the coherent structures of counter-rotating streamwise Görtler vortices on erosion and bed form evolution, using a coupled bed-flowfield numerical model based on Paik et al. (2007) and Escauriaza and Sotiropoulos (2011a, 2011b, 2009) formulation for fixed bed simulations explained before. The proposed model solves numerically the three-dimensional, unsteady, Reynolds-averaged Navier-Stokes equations using the so-called Arbitrary Lagrangian-Eulerian (ALE) approach coupled with a new bed-load transport equation that uses the instantaneous flowfield -solved in previous sections- to predict the sediment flux used in Exner equation. According to the computations obtained from the flowfield and sediment transport model employed, the simulations show sediment streaks produced by Görtler vortices as is shown

in figure 6.1 and how it was reported in the experiments of Hopfinger et al. (2004). The model is capable not only to reproduce these streaks but is capable to reproduce little ripples that appears on results of experiences of Hopfinger et al. (2004). These features are related to the increase of shear stress at the bed zone since the high values of shear velocity, presented in the previous section, are located at the same zone ($6 < X/b < 9$). Is important to note that these sediment transport simulations are intents to reproduce the same qualitative features of the experiments carried out by Hopfinger et al. (2004) and Albayrak et al. (2008), quantitative analyses could be carried out in a future research. Furthermore, the model is a tool to reproduce the bed sediment transport, and is not capable to reproduce saltation and suspention of sediment particles observed in experiments of Hopfinger et al. (2004) and Albayrak et al. (2008).

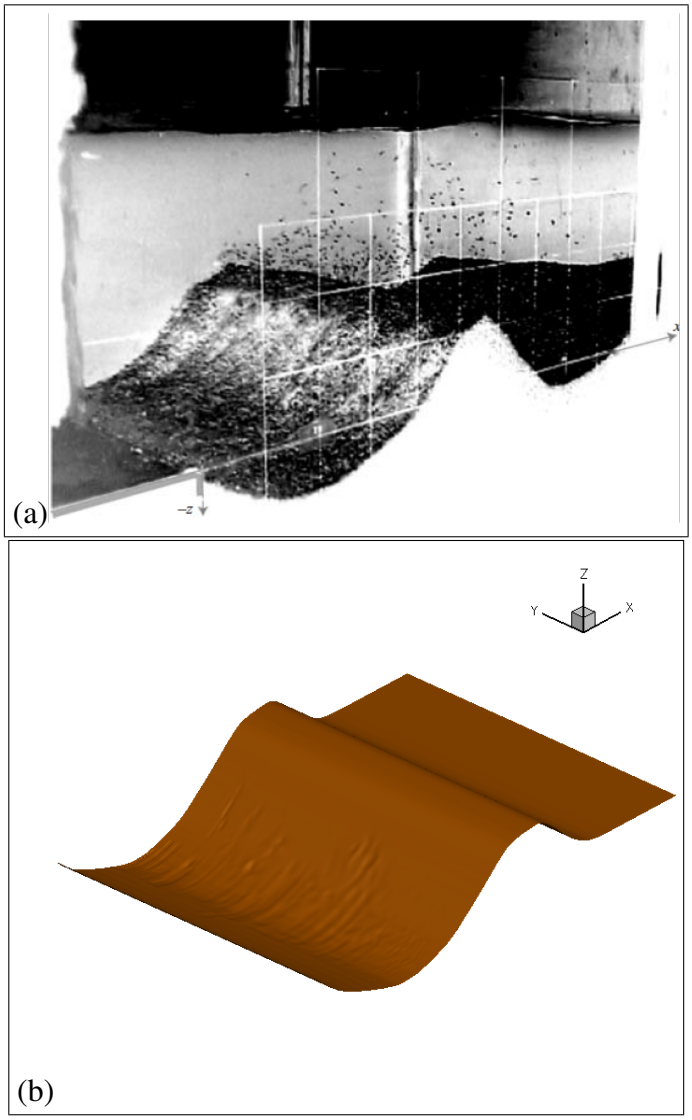

FIGURE 6.1. (a) Sediment streak patterns reported by Hopfinger *et al*. (2004). (b) Instantaneous image of the initial stage of the scour-bed obtained from sediment transport simulations. The model is capable to represent the sediment patterns reported in experiments and explains the relation between the increase of shear-stress produced by the appearance of Görtler vortices in the scour-hole region.

7. CONCLUSIONS AND FUTURE RESEARCH

In this investigation we perform numerical simulations of the flow downstream a submerged sluice gate over a rough concave bed at $Re = 156,200$. We reproduce the configuration of the scour experiments carried out by Albayrak et al. (2008).

The flow is characterized by a wide range of time and length scales, dominated by unsteady coherent structures induced by the complex geometry of the domain and the wall-jet coming from sluice gate. DES simulations shows that our model successfully captures the dynamic features of the coherent structures within the scour hole, and the formation of Görtler vortices near the bed. Pairs of highly unsteady counter-rotating streamwise vortices appear inside the scoured region, forming mushroom-like structures that have been reported in multiple studies of turbulent boundary layer flows over concave surfaces. Animations of q-isosurfaces showed that inside the scoured region the flow is dominated by the shear-layer produced by the wall-jet that emanates from the flat-bed channel. These horizontal structures exhibit significantly smaller time-scales compared to the Görtler vortices. On the other hand, pairs of streamwise structures, identified as counter-rotating Görtler vortices, occupy a significant portion of the bed within the scour hole. They appear intermittenly and move laterally with low frequencies as reported by Albayrak et al. (2008). Furthermore, the computation demonstrated that Görtler vortices also developed over a smooth wall indicating that surface roughness is not a prerequisite to trigger the instability in this flow. Other important finding obtained from the DES computations is that the Görtler vortices develop in both directions from the reattachment point, as it is shown in section 4. After the wall-jet reattaches to the sand bed, Görtler vortices form in opposite directions inside the recirculation vortex near the wall, and on the upslope face to the dune.

We also reproduce quantitative experimental results reported by Hopfinger et al. (2004) and Albayrak et al. (2008). Plots of instantaneous shear velocity at the bed show that Görtler vortices are directly responsible for the increase of bed stresses, and consequently for the larger sediment transport rates that were observed by Hopfinger et al. (2004). The simulations capture statistically the same upwash and downwash flow events reported by

Albayrak et al. (2008) with similar time-scales, including the increments of instantaneous Reynolds stresses obtained from resolved velocity fluctuations. In addition, a sediment transport model was applied for modeling the sediment streaks reported by Hopfinger et al. (2004). This model is capable to represent qualitatively the patterns founded in experiments, which is explained by the effects on shear-stress increase produced by the appearance of Görtler vortices in the scoured zone.

The model capture in detail the dynamics of the Görtler vortices in this complex flow. This information is critical to employ new methods to determine bed-load transport and scour induced by turbulent coherent structures. Future research must include sediment transport statiscal analyses, to show in a better way the effects of the coherent-structures on the scour process.

REFERENCES

Aihara, Y. (1976). Nonlinear analysis of Görtler vortices. *Phys. Fluids*, *19*, 1655–1660.

Albayrak, I., Hopfinger, E. J., & Lemmin, U. (2008). Near-field flow structure of a confined wall jet on flat and concave rough walls. *J. Fluid Mech.*, *606*, 27–49.

Aupoix, B., & Spalart, P. R. (2003). Extensions if the spalart-allamaras turbulence model to acount for wall roughness. *Int. J. Heat Fluid Flow*, *24*, 454–462.

Auton, T. R. (1987). The lift force on a spherical body in a rotational flow. *J. Fluid Mech.*, *183*, 199–218.

Auton, T. R., Hunt, J. C. R., & Prud'homme, M. (1988). The force exerted on a body in inviscid unsteady non-uniform rotational flow. *J. Fluid Mech.*, *197*, 241–257.

Bagnold, R. A. (1956). The flow of cohesionless grains in fluids. *Phil. Trans. Royal Soc. London A*, *225*, 49–63.

Bagnold, R. A. (1973). The nature of saltation and of 'bed-load' transport in water. *Proc. Royal Soc. London A*, *332*, 473–504.

Boivin, M., Simonin, O., & Squires, K. D. (2000). On the prediction of gas-solid flows with two-way coupling using large eddy simulation. *Phys. Fluids*, *12*, 2080–2090.

Burton, T. M., & Eaton, J. K. (2005). Fully resolved simulations of particle-turbulence interaction. *J. Fluid Mech.*, *545*, 67–111.

Chang, Y. S., & Scotti, A. (2003). Entrainment and suspension of sediments into a turbulent flow over ripples. *J. Turbul.*, *4*, 019.

Chang, Y. S., & Scotti, A. (2004). Modeling of unsteady turbulent flows over ripples: Reynolds-averaged Navier-Stokes (RANS) versus large-eddy simulation LES. *J. Geophys. Res*, *109*, C09012.

Chang, Y. S., & Scotti, A. (2006). Turbulent convection of suspended sediments due to flow reversal. *J. Geophys. Res*, *111*, C07001.

Crowe, C. T., Sommerfeld, M., & Tsuji, Y. (1998). *Multiphase flows with droplets and particles*. CRC Press LLC.

Crowe, C. T., Troutt, T. R., & Chung, J. N. (1996). Numerical models for two-phase turbulent flows. *Annu. Rev. Fluid Mech.*, *28*, 11–43.

Drew, D. A. (1983). Mathematical modeling of two-phase flow. *Annu. Rev. Fluid Mech.*, *15*, 261–291.

Durbin, P. A., & Petterson-Reif, B. A. (2001). *Statistical theory and modeling for turbulent flows*. New York: John Wiley & Sons.

Engelund, F., & Fredsøe, J. (1976). A sediment transport model for straight alluvial channels. *Nordic Hydrol.*, *7*, 293–306.

Engelund, F., & Hansen, E. (1967). *A monograph on sediment transport to alluvial streams*. Denmark: Copenhagen: Teknik Vorlag.

Escauriaza, C. (2008). *Three-dimensional unsteady modeling of clear-water scour in the vicinity of hydraulic structures: Lagrangian and Eulerian perspectives*. Unpublished doctoral dissertation, University of Minnesota.

Escauriaza, C., & Sotiropoulos, F. (2009). Trapping and sedimentation of inertial particles in three-dimensional flows in a cylindrical container with exactly counter-rotating lids. *J. Fluid Mech.*, *641*, 169-193.

Escauriaza, C., & Sotiropoulos, F. (2011a). Initial stages of erosion and bed-form development in a turbulent flow around a cylindrical pier. *accepted for publication in J. Geophys. Res.*

Escauriaza, C., & Sotiropoulos, F. (2011b). Lagrangian model of bed-load transport in turbulent junction flows. *J. Fluid Mech.*, *666*, 36-76.

Escauriaza, C., & Sotiropoulos, F. (2011c). Reynolds number effects on the coherent dynamics of the turbulent horseshoe vortex system. *Flow Turbul. Combust.*, *86*, 231-262.

Floryan, J. M. (1986). Görtler instability of boundary layers over concave and convex walls. *Phys. Fluids*, *29*, 2380–2387.

Ge, L., & Sotiropoulos, F. (2005). 3D Unsteady RANS modeling of complex hydraulic engineering flows. Part I: Numerical Model. *J. Hydraul. Eng.*, *131*, 800–808.

Görtler, H. (1954). *On the three-dimensional instability of laminar boundary layers on concave walls*. National Advisory Committee For Aeronautics.

Hall, P. (1988). The nonlinear development of Görtler vortices in growing boundary layers. *J. Fluid Mech.*, *193*, 243-266.

Hall, P. (1990). Görtler vortices in growing boundary layers: The leading edge receptivity problem, linear growth and the nonlinear breakdown stage. *Mathematika*, *37*, 151-189.

Hogg, A. J., Huppert, H. E., & Dade, W. B. (1997). Erosion by planar turbulent wall jets. *J. Fluid Mech.*, *338*, 317-340.

Hopfinger, E. J., Kurniawan, A., Graf, W. H., & Lemmin, U. (2004). Sediment erosion by Görtler vortices: The scour-hole problem. *J. Fluid Mech.*, *520*, 327–342.

Hu, G., & Celik, I. (2008). Eulerian-Lagrangian based large-eddy simulation of a partially aerated flat bubble column. *Chem. Eng. Sci.*, *63*, 253–271.

Hunt, J. C. R., Wray, A. A., & Moin, P. (1988). Eddies, stream, and convergence zones in turbulent flows. In *Proceedings of the summer program.* Center for Turbulence Research, NASA Ames/Stanford Univ., pages 193-208.

Kobayashi, R., & Fujisawa, N. (1983). Turbulence measurements in wall jets along strongly concave surfaces. *Acta Mech.*, *47*, 39-52.

Kovacs, A., & Parker, G. (1994). A new vectorial bedload formulation and its application to the time evolution of straight river channels. *J. Fluid Mech.*, *267*, 153–183.

Lakehal, D. (2002). On the modelling of multiphase turbulent flows for environmental and hydrodynamic applications. *Int. J. Multiphase Flow*, *28*, 823–863.

Loth, E. (2000). Numerical approaches for motion of dispersed particles, droplets, and bubbles. *Prog. Energy Combust. Sci.*, *26*, 161–223.

Matsson, O. J. E. (1995). Experiments on streamwise vortices in curved wall jet flow. *Phys. Fluids*, *7*, 2978.

Maxey, M. R., Patel, B. K., Chang, E. J., & Wang, L. P. (1997). Simulations of dispersed turbulent multiphase flow. *Fluid Dyn. Res.*, *20*, 143–156.

Maxey, M. R., & Riley, J. J. (1983). Equation of motion for a small rigid sphere in a non-uniform flow. *Phys. Fluids*, *26*, 883–889.

Mei, R. (1992). An approximate expression for the shear lift force on a spherical particle at finite Reynolds number. *Int. J. Multiphase Flow*, *18*, 145–147.

Melville, B. W. (1997). Pier abutment scour: Integrated approach. *J. Hydraul. Eng.*, *123*, 125–136.

Michaelides, E. E. (2003). Hydrodynamic force and heat/mass transfer from particles, bubbles, and drops. *J. Fluids Eng.*, *125*, 209–238.

Nadaoka, K., Nihei, Y., & Yagi, H. (1999). Grid-averaged Lagrangian LES model for multiphase turbulent flow. *Int. J. Multiphase Flow*, *25*, 1619–1643.

Niño, Y., Atala, A., Barahona, M., & Aracena, D. (2002). Discrete particle model for analyzing bedform development. *J. Hydraul. Eng.*, *128*, 381.

Paik, J., Escauriaza, C., & Sotiropoulos, F. (2007). On the bimodal dynamics of the turbulent horseshoe vortex system in a wing-body junction. *Phys. Fluids*, *19*, 045107.

Paik, J., Escauriaza, C., & Sotiropoulos, F. (2010). Coherent structure dynamics in turbulent flows past in-stream structures: Some insights gained via numerical simulation. *J. Hydraul. Eng.*, *136*, 981-993.

Paik, J., Ge, L., & Sotiropoulos, F. (2004). Toward the simulation of complex 3D shear flows using unsteady statistical turbulence models. *Int. J. Heat Fluid Fl.*, *25*, 513–527.

Paik, J., & Sotiropoulos, F. (2005). Coherent structure dynamics upstream of a long rectangular block at the side of a large aspect ratio channel. *Phys. Fluids*, *17*, 115104.

Paik, J., & Sotiropoulos, F. (2009). Numerical simulations of strongly swirling turbulent flow through an abrupt expansion. *In press Int. J. Heat Fluid Fl.*, *31*, 390-400.

Paik, J., Sotiropoulos, F., & Porté-Agel, F. (2009). Detached eddy simulation of the flow around two wall-mounted cubes in tandem. *Int. J. Heat Fluid Fl.*, *30*, 286-305.

Paola, C., & Voller, V. R. (2005). A generalized Exner equation for sediment mass balance. *J. Geophys. Res*, *110*, F04014.

Parker, G., Seminara, G., & Solari, G. (2003). Bedload at low shields stress on arbitrarily sloping beds: Alternative entrainment formulation. *Water Resour. Res.*, *39*, 1183.

Pope, S. B. (2000). *Turbulent flows*. Cambridge University Press.

Ragab, S. A., & Nayfeh, A. H. (1981). Görtler instability. *Phys. Fluids*, *8*, 081405.

Rintel, L. (1971). Görtler instability of boundary layers. *Phys. Fluids*, *14*, 753–759.

Roulund, A., Sumer, B. M., Fredsøe, J., & Michelsen, J. (2005). Numerical and experimental investigation of flow and scour around a circular pile. *J. Fluid Mech.*, *534*, 351–401.

Saffman, P. (1965). The lift on a small sphere in a slow shear flow. *J. Fluid Mech.*, *22*, 385–400.

Saffman, P. (1968). Corrigendum to the lift on a small sphere in a slow shear flow. *J. Fluid Mech.*, *31*, 624.

Saric, W. (1994). Görtler vortices. *Annu. Rev. Fluid Mech.*, *26*, 379–409.

Schmeeckle, M. W., Nelson, J. M., Pitlick, J., & Bennett, J. P. (2001). Interparticle collision of natural sediment grains in water. *Water Resour. Res.*, *37*, 2377–2391.

Schweizer, P. M., & Scriven, L. E. (1983). Evidence of Görtler-type vortices in curved film flows. *Phys. Fluids*, *26*, 030619.

Shur, M., Spalart, P. R., Strelets, M., & Travin, A. (1999). Detached-eddy simulation of an airfoil at high angle of attack. In W. Rodi & D. Laurence (Eds.), *Turbulent shear flows* (pp. 669–678). Elsevier Science, Amsterdam.

Sotiropoulos, F., & Abdallah, S. (1992). A primitive variable method for the solution of 3D, incompressible, viscous flows. *J. Comput. Phys.*, *103*, 336–349.

Sotiropoulos, F., & Constantinescu, G. (1997). Pressure-based residual smoothing operators for multistage pseudocompressibility algorithms. *J. Comput. Phys.*, *133*, 129–145.

Spalart, P. R. (2000). Strategies for turbulence modeling and simulations. *Int. J. Heat Fluid Fl.*, *21*, 252–263.

Spalart, P. R. (2009). Detached-eddy simulation. *Annu. Rev. Fluid Mech.*, *41*, 181–202.

Spalart, P. R., & Allmaras, S. R. (1994). A one-equation turbulence model for aerodynamic flows. *Rech. Aerosp.*, *1*, 5-21.

Spalart, P. R., Jou, W. H., Strelets, M., & Allmaras, S. R. (1997). Comments on the feasibility of LES for wings and on a hybrid RANS/LES approach. In C. Liu & Z. Liu (Eds.), *Advances in DNS/LES.* Greyden Press, Columbus OH.

Squires, K. D., Forsythe, J. R., & Spalart, P. R. (2005). Detached-eddy simulation of the separated flow over a rounded-corner square. *J. Fluids Eng.*, *127*, 959–966.

Tandiono, Winoto, S., & Shah, D. (2008). On the linear and nonlinear development of Görtler vortices. *Phys. Fluids.*, *20*, 094103.

Tandiono, Winoto, S., & Shah, D. (2009). Wall shear stress in Görtler vortex boundary layer flow. *Phys. Fluids.*, *21*, 084106.

Tani, I. (1962). Production of longitudinal vortices in the boundary layer along a concave wall. *J. Geophys. Res.*, *67*, 3075-3080.

Wiberg, P. L., & Smith, J. D. (1985). A theoretical model for saltating grains in water. *J. Geophys. Res.*, *90*, 7341–7354.

Wu, W., Rodi, W., & Wenka, T. (2000). 3D numerical model of flow and sediment transport in open channels. *J. Hydraul. Eng.*, *126*, 4–15.

Zebib, A., & Bottaro, A. (1993). Goertler vortices with system rotation: Linear theory. *Phys. Fluids*, *5*, 051206.